Bone ingrowth in a shoulder prosthesis
MSC Thesis, Applied Mathematics

E.M.van Aken

1107895

emvanaken@hotmail.com

Delft, September 4th 2007

Contents

Acknowledgments

I would like to thank the numerical department of the TU Delft, especially my supervisor dr. ir. Fred Vermolen. He has helped me during the whole time, answering my questions and giving comments.

Further I would like to thank dr. ir. Jacqueline van der Linden, for helping me and for making it possible to work at Erasmus MC for a few weeks. I also want to thank Daniel, for answering my questions and showing me around at the lab at LUMC, and Ruud, for showing the lab at Erasmus MC.

My gratitude also goes to Dori Steeneken for providing me a place to work at the TU.

Further, I would like to thank my friends (in alphabetic order) Floris, Jalitha and Pim for their help, especially with Latex. Because of them the actual writing of the report became a lot less difficult. I want to thank my roommate-for-a-few-months Jan-Willem, Bert-Jan and my brother Krijn for answering questions, my sister Annet for lending me some books about human anatomy and I should not forget Petra, who dropped by several times so i could get my mind off work for some time.

Further my gratitude also goes to prof. dr. ir. Kees Vuik and dr. Henk Schuttelaars for being part of the graduation committee.

Chapter 1

Introduction

As a result of osteoporosis, osteoarthritis, rheumatoid arthritis or severe trauma from a shoulder fracture, it is possible that the shoulder joint dysfunctions. The cartilage is thinner than it is supposed to be or the bones are too weak. As a result the bones rub together causing pain, swelling and/or loss of motion of the joint. To improve the movement of the joint and to relieve the pain, a prosthesis to replace the glenoid of the shoulder joint is an option.

The shoulder is a so called ball-and-socket joint [1]. In ball-and-socket joints the spherical of hemispherical head of one bone articulates with the cup-like socket of another. These joints are multiaxial and the most freely moving synovial joints. Moving is allowed in all axes and planes, including rotation.
In the shoulder joint, stability has been sacrificed to provide the most freely moving joint of the body. The large hemispherical head of the humerus fits in the small glenoid cavity of the scapula (shoulder blade), see Figure 1.1.
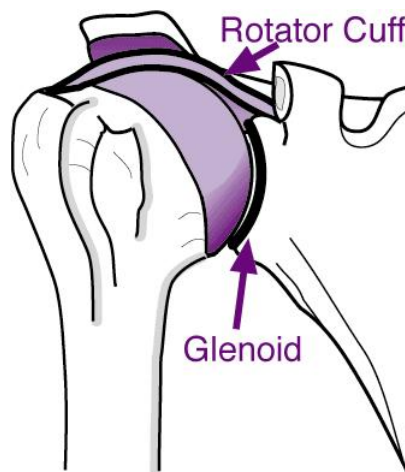
Figure 1.1: The shoulder joint is a ball-and-socket joint [2].

The range of motion of the joint is determined by the rate of coverage of the ball by the socket. In the shoulder joint the glenoid cavity is only about one-third of the size of the humeral head, so it provides a large range of motion, but little joint stability.

Before the prosthesis is placed, the cartilage will be removed from the glenoid cavity, so the prosthesis will have direct contact to the bone. The prosthesis, often made of stainless steal combined with polyethylene, replaces this glenoid cavity and is made of porous material at the bone side, see Figure 1.2. This way bone can grow into the prosthesis, which leads to a fusion of bone and prosthesis.

According to Wolff's law [1], it is possible that no bone ingrowth will occur at all, if the mechanical stress is too low. The anatomy of a bone reflects the common stresses it encounters. A bone is loaded whenever weight bears down on it or muscles pull on it. Since this loading is usually off-center, it tends to bend the bone. Deforming of the bone produces an electrical current which signals the cells responsible for bone modeling. One can speculate that the hormonal loop determines *whether* and *when* bone remodeling occurs (in response to changing blood calcium levels), and mechanical stress determines *where* it occurs. For this reason it is important to know what the stress

Figure 1.2: The glenoid replacement is made of polyethylene or stainless steel [3].

distribution should be and what material is best to be used for the prosthesis, to make sure the bone ingrowth is optimal. With that information then it can be determined, what exercises should be done after joint replacement to provide optimal growth, see Figure 1.3.

The model to simulate the bone ingrowth consists of two parts: one part relating to the biophysical stimuli and the other part relating to the tissue differentiation. In this report the tissue differentiation will be discussed by using two different models.
Chapter 2 explains the cell differentiation process, which is similar to the process of secondary healing of a bone fracture. Several models describing this process will be discussed. For two models the differential equations will be given and boundary conditions will be derived.
The models can be solved using numerical methods. The Finite Element Method discretisation is used in this report and will be shown for the differential equations of the biological part of the model due to Prendergast in Chapter 3. This has been implemented to get a solution.
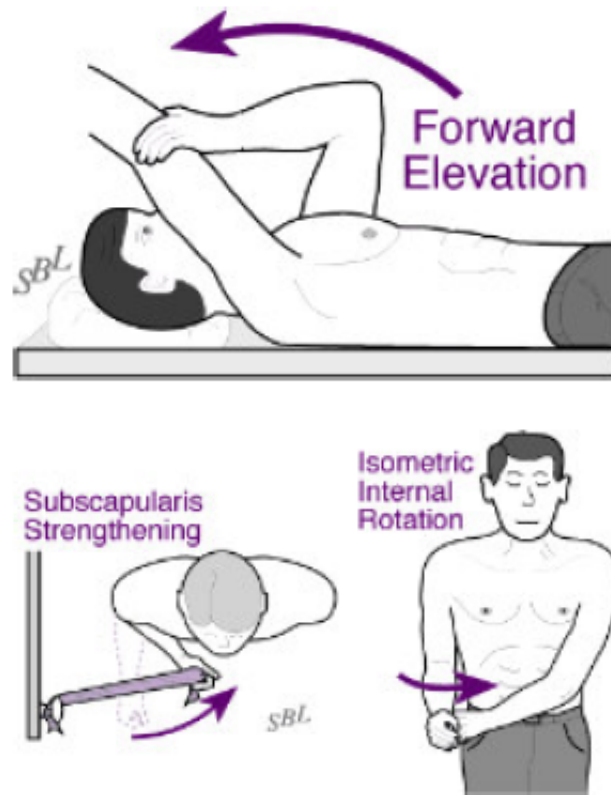
Figure 1.3: Exercises to be done after surgery [2].

In Chapter 4 the results will be given and also a sensitivity analysis is performed.

Chapter 5 discusses the discretisation of the model due to Bailon-Plaza, using the Finite Element Method, and the results of this model are shown in Chapter 6. The mechanical part of the Prendergast model will be derived in Chapter 7 and in Chapter 8 the discretisation of the equations will be shown.

The biological part, which was already handled in Chapter 3, and the mechanical part of the model due to Prendergast is implemented and simulated together. The results are shown in Chapter 9.

All simulations in this report are performed with MATLAB.

In chapter 10 some conclusions are drawn and some recommendations will be given.

Chapter 2

Models of tissue differentiation

The cell differentiation during bone ingrowth in an artificial shoulder is actually the same process as the cell differentiation during a secondary fracture healing. Fracture healing begins as undifferentiated mesenchymal cells migrate from the periosteum and the surroundings (like muscles). They produce initial connective tissue around the fracture side, forming an initial stabilizing callus [4]. This callus depends on the size of the fracture gap and the mechanical stability.

Healing processes can be divided into two groups: primary healing and secondary healing. Primary healing takes place when the fracture size is very small and stable. The bone fragments get reattached by direct bone remodeling, forming a very small or no callus.

In most cases fractures heal by secondary healing. This happens when the fracture size is relatively big or unstable. Secondary healing can be divided into four stages [4] [1]: Inflammation, callus differentiation, ossification and remodeling, see Figure 2.1.

Stage 1: Inflammation. During the inflammation stage blood cells, coming from the ruptured blood vessels, form a fibrin matrix. Mesenchymal cells originate from the broken periosteum and replace the fibrin matrix to form the external callus.

Depending on the mechanical and biological environment the mesenchymal cells differentiate into fibroblast (cells forming fibrous tissue), chondrocytes (cartilage-forming cells) or osteoblast (bone-forming cells).

Stage 2: Callus differentiation. During callus differentiation mesenchymal cells along the bone side differentiate into osteoblasts, which begin to actively synthesize intra-membranous woven bone. In the interior of the callus mesenchymal cells differentiate into chondrocytes, while mesenchymal cells that reach the fracture gap will differentiate into fibroblasts.

Stage 3: Ossification. During healing the intra-membranous ossification front advances towards the center of the callus and the chondrous callus grows due mesenchymal cell differentiation into chondrocytes and chondrocytic prolifera-
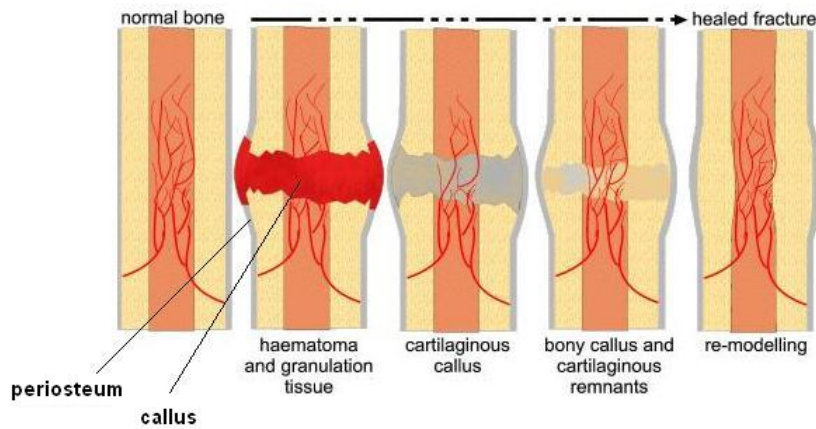
Figure 2.1: The different stages during the process of bone fracture healing [5].

tion. As time goes on ossification of the cartilage callus starts, called endochondral ossification.

During endochondral ossification chondrocytes undergo apoptosis and will be replaced with osteoblasts. This process continues until all the cartilage is replaced with bone and the fracture gap is closed.

Stage 4: Bone remodeling. The excess material within the cavity is removed and compact bone is laid down to reconstruct the original form of the bone. The final structure resembles the original unbroken bony region, because it responds to the same mechanical stressors. This last stage has not been studies in the models presented here.

2.1 Model due to Prendergast

The first model to be discussed with is the model due to Prendergast. This model describes the behavior of the mesenchymal cells, the fibroblasts, the chondrocytes and the osteoblasts and also the matrix production caused by these various cell types [6].

Since it is assumed that the mesenchymal cells and the fibroblasts migrate through the callus, they are modeled by means of a diffusion-reaction equation. The chondrocytes and the osteoblasts are assumed not to migrate, so their equations do not contain diffusion terms.

For all these cell types there is one term that describes the proliferation of the cell type and one or more terms to describe the differentiation of the cells (see Figure 2.2). For example the mesenchymal cells can differentiate into fibroblasts, chondrocytes or osteoblasts, so the equations for the mesenchymal cells contains three differentiation terms. The matrix densities are influenced by the production and resorption rates of the various tissues and the cellular densities of the corresponding tissue. The resorption rates are chosen to be equal to the production rates.
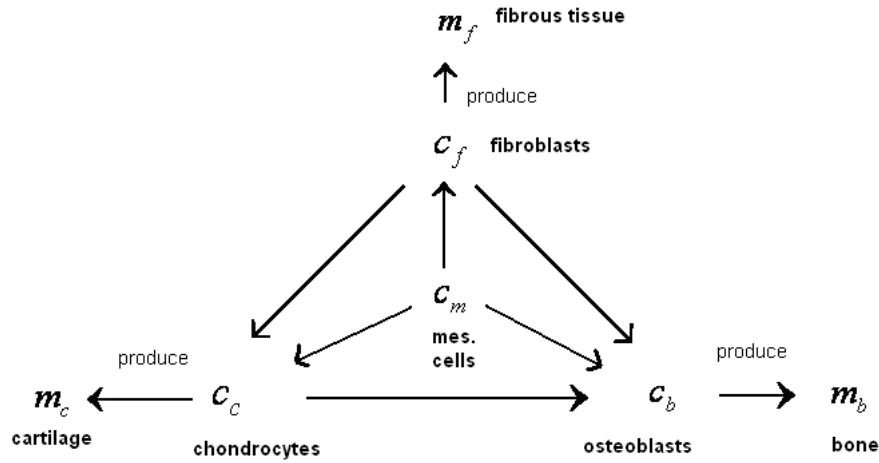
Figure 2.2: Mesenchymal cells can differentiate into fibroblasts, chondrocytes or osteoblasts. Fibroblasts can differentiate into chondrocytes and osteoblasts. Chondrocytes can differentiate into osteoblasts.

The following symbols will be used:

c_m the mesenchymal cellular density,
c_f the fibroblast density,
c_c the chondrocyte density,
c_b the osteoblast density,
and $c_{tot} = c_m + c_c + c_b + c_f$.
m_f the fibrous matrix density,
m_c the cartilage matrix density,
m_b the bone matrix density,
and $m_{tot} = m_c + m_b + m_f$.
D_m the diffusion coefficient of the mesenchymal cells and
D_f the diffusion coefficient of the fibroblasts,
(depending on m_f, m_c and m_b).
P_i the proliferations rates, for $i = m, f, c, b$,
F_i the differentiation rates, for $i = f, c, b$,
Q_i the production rates of the tissue(matrix), for $i = f, c, b$,
D_i the tissue resorption rates (equal to Q), for $i = c, b$.

For the proliferation rates and the differentiation rates, the subscript i refers to either mesenchymal cells (m), fibroblasts (f), chondrocytes (c) or osteoblasts (b). For the production and resorption rates the index i refers to either fibrous tissue (f), cartilage (c) or bone (b).

Initially the callus is only filled with granulation tissue and all the cell

concentrations are zero. Thus the initial conditions are given by

$$c_i(\underline{x}, 0) = m_i(\underline{x}, 0) = 0.$$

Mesenchymal cells originate from the periosteum layer and the bone marrow. Hence the mesenchymal cell density at those areas is kept constant at the highest saturation level, thus

$$c_m|_{periosteum} = c_{max}, \forall t.$$

The change in the cellular densities can be described by the following partial differential equations:

$$
\begin{aligned}
\frac{\partial c_m}{\partial t} &= \nabla \cdot (D_m \nabla c_m) + P_m(1 - c_{tot})c_m - F_f(1 - c_f)c_m - F_c(1 - c_c)c_m \\
&\quad -F_b(1 - c_b)c_m, \tag{2.1} \\
\frac{\partial c_f}{\partial t} &= \nabla \cdot (D_f \nabla c_f) + P_f(1 - c_{tot})c_f + F_f(1 - c_f)c_m - F_c(1 - c_c)c_f \\
&\quad -F_b(1 - c_b)c_f, \tag{2.2} \\
\frac{\partial c_c}{\partial t} &= P_c(1 - c_{tot})c_c + F_c(1 - c_c)(c_m + c_f) - F_b(1 - c_b)c_c, \tag{2.3} \\
\frac{\partial c_b}{\partial t} &= P_b(1 - c_{tot})c_b + F_b(1 - c_b)(c_m + c_f + c_c). \tag{2.4}
\end{aligned}
$$

The first terms on the right hand side of (2.1) and (2.2) represent the diffusion of the mesenchymal cells and the fibroblasts respectively. The second terms in (2.1) and (2.2) represent the proliferation of the cells. The last three terms of (2.1) express the differentiation from mesenchymal cells into fibroblasts, chondrocytes and osteoblasts. These last terms will come back in the equations for the other cell types.
The third term of (2.2) represents the cells which differentiate from mesenchymal cells into fibroblasts. The fourth and fifth term of (2.2) represent the differentiation of fibroblasts into chondrocytes and osteoblasts.
The equations for chondrocyte density (2.3) and osteoblast density (2.4) only contain terms for proliferation and differentiation.

The change in the matrix densities is given by the following differential equations:

$$
\begin{aligned}
\frac{\partial m_f}{\partial t} &= Q_f(1 - m_{tot})c_f - (D_b c_b + D_c c_c)m_f m_{tot}, \tag{2.5} \\
\frac{\partial m_c}{\partial t} &= Q_c(1 - m_b - m_c)c_c - D_b c_b m_c m_{tot}, \tag{2.6} \\
\frac{\partial m_b}{\partial t} &= Q_b(1 - m_b)c_b. \tag{2.7}
\end{aligned}
$$

The first terms on the right-hand-side of (2.5), (2.6) and (2.7) express the production of the tissue. The second terms on the right hand side of (2.5) and (2.6) represent the resorption of the tissue.

Cell differentiation, proliferation and tissue production are regulated by

tissue shear strain and interstitial fluid velocity, so P, F, Q depend on S. The following equation holds for S:

$$S = \frac{\gamma}{a} + \frac{\nu}{b}, \tag{2.8}$$

where γ represents the maximum shear strain and ν the fluid/solid velocity. This will be discussed in Chapter 7.

2.2 Model due to Bailon-Plaza

Another model that is investigated is the model due to Bailon-Plaza [4]. This model does not take the fibroblasts and the fibrous tissue into account and has some additional equations for the growth factors of bone and cartilage .
Growth factors are hormones that are involved in cell differentiation and growth [7]. So they influence the differentiation rates from mesenchymal cells into either osteoblasts or chondrocytes and the endochondral replacement of the chondrocytes. Unlike the previous model, where the growth factors themselves are not modeled, this models behavior is described by means of a convection-diffusion-reaction equation. So they are assumed to migrate and they are depending on their corresponding cellular densities and the growth factor production rates.
For the mesenchymal cells, chondrocytes and osteoblasts and the bone and cartilage matrix densities the same sort of equations are chosen as in the previous model.
The equations for the change in mesenchymal, cartilage and bone cell densities are

$$\frac{\partial c_m}{\partial t} = \nabla \cdot (D\nabla c_m - Cc_m \nabla m) + A_m c_m (1 - \alpha_m c_m) - F_1 c_m - F_2 c_m \tag{2.9}$$

$$\frac{\partial c_c}{\partial t} = A_c c_c (1 - \alpha_c c_c) + F_2 c_m - F_3 c_c, \tag{2.10}$$

$$\frac{\partial c_b}{\partial t} = A_b c_b (1 - \alpha_b c_b) + F_1 c_m + F_3 c_c - d_b c_b, \tag{2.11}$$

where D and C represent the haptotactic and haptokinetic cell migration speeds. The proliferation rates are denoted by A_m, A_c and A_b, further F_1 is the mesenchymal differentiation into osteoblasts, F_2 the mesenchymal differentiation into chondrocytes and F_3 the endochondral replacement of chondrocytes. The symbol d_b stands for osteoblasts removal and the α_i's result from non-dimensionalizing the equations. Furthermore it holds: $m = m_c + m_b$.
The changes in cartilage and bone matrix densities are modeled in the following way:

$$\frac{\partial m_c}{\partial t} = P_{cs}(1 - \kappa_c m_c)(c_m + c_c) - Q_{cd} m_c c_b, \tag{2.12}$$

$$\frac{\partial m_b}{\partial t} = P_{bs}(1 - \kappa_b m_b)c_b, \tag{2.13}$$

where P_{cs} and P_{bs} represent constants of cartilage and bone matrix production and Q_{cd} is a constant of matrix degradation.

The growth factor concentrations g_c and g_b are modeled in the following way:

$$\frac{\partial g_c}{\partial t} = \nabla \cdot (D_{gc} \nabla g_c) + E_{gc} c_c - d_{gc} g_c, \qquad (2.14)$$

$$\frac{\partial g_b}{\partial t} = \nabla \cdot (D_{gb} \nabla g_b) + E_{gb} c_b - d_{gb} g_b, \qquad (2.15)$$

where D_{gc} and D_{gb} are diffusion coefficients, E_{gc} and E_{gb} are functions relating growth factor production to growth factor concentration, and d_{gc} and d_{gb} are constants of decay.

The initial and boundary conditions for the cellular densities and the matrix densities are given by

$$c_m\big|_{periosteum} = c_{max}, \quad \frac{\partial c_m}{\partial x}\bigg|_{other\ boundaries} = 0, \quad \forall t,$$

$$c_m(\underline{x}, 0) = 0, \qquad c_c(\underline{x}, 0) = 0, \qquad c_b(\underline{x}, 0) = 0.$$

$$m_b(\underline{x}, 0) = 0, \qquad m_c(\underline{x}, 0) = 0.1.$$

The initial and boundary conditions for the growth factors are given by

$$g_i(\underline{x}, 0) = 0, \qquad \text{where } i = c, b.$$

For $t \leq t_K$

$$g_c\big|_{fracture\ gap} = 20, \quad g_b\big|_{along\ bone} = 20, \quad \frac{\partial g_i}{\partial x}\bigg|_{other\ boundaries} = 0.$$

For $t > t_K$

$$\frac{\partial g_i}{\partial x}\bigg|_{all\ boundaries} = 0, \qquad \text{where } i = c, b.$$

t_K is the time after which no growth factors will originate anymore from the fracture gap and along the bone respectively.

Finally the functions are defined by:

$$D = \frac{D_h}{(K_h^2 + m^2)}m,$$

$$C = \frac{C_k}{(K_k + m)^2},$$

$$A_m = \frac{A_{m0}}{(K_m^2 + m^2)}m,$$

$$A_c = \frac{A_{c0}}{(K_c^2 + m^2)}m,$$

$$A_b = \frac{A_{b0}}{(K_b^2 + m^2)}m,$$

$$F_1 = \frac{Y_1}{(H_1 + g_b)}g_b,$$

$$F_2 = \frac{Y_2}{(H_2 + g_c)}g_c,$$

$$F_3 = (\frac{m_c^6}{B_{ec}^6 + m_c^6})(\frac{Y_3}{H_3 + g_b})g_b,$$

$$E_{gc} = (\frac{G_{gc}g_c}{H_{gc} + g_c})(\frac{m}{K_{gc}^3 + m^3}),$$

$$E_{gb} = \frac{G_{gb}g_b}{(H_{gb} + g_b)},$$

where D_h, K_h,C_k, K_k, A_{m0}, K_m, A_{c0}, K_c, A_{b0}, K_b, Y_1, H_1, Y_2, H_2, Y_3, H_3, B_{ec}, G_{gc}, H_{gc}, K_{gc}, G_{gb} and H_{gb} are constants.
The functions and constants are not regulated by a mechanical stimulus. Hence, in the model due to Bailon-Plaza, no mechanical stresses and strains have been taken into account.

2.3   Other models

2.3.1   Model due to Ament and Hofer

Another model for fracture healing is the model due to Ament and Hofer [8]. It is an algorithm which also consist of a mechanical stimuli part and a tissue differentiation part, only here both should be determined during every time step. The three types of tissues that are involved here are: cartilage, bone and fibrous connective tissue. The latter contains also granulation tissue in this model. It is assumed that each element is completely composed by these three types of tissue.

At every time step should, for each element, be looked at the dominating part of the tissue composition, to figure out if it is fibrous tissue, cartilage or bone.
The strain energy density can be determined using the Young modulus and the Poisson ratio. The tissue differentiation is determined by the spatial change

of the bone matrix density. This is called the osteogenic factor. This will be calculated for every element.

Finally, when both the strain energy density and the osteogenic factor are determined, the tissue differentiation rates per element are calculated, which leads to the new tissue composition.

2.3.2   Model due to Adam

The model due to Adam [9] examines the conditions under which wound healing will occur. A thin layer of bone at the wound edges manufactures growth factors. In 1-D these layers is positioned at $-L/2-\delta \leq x \leq -L/2$ and $L/2 \leq x \leq L/2+\delta$. The wound width is located at $-L/2 \leq x \leq L/2$.

Since this problem is symmetric from now on only the domain $[0,\infty)$ will be considered. The goal is to find a value for δ, so healing will occur.

The fundamental equation for the growth factor concentration is described by

$$\frac{\partial C}{\partial t} = D\frac{\partial^2 C}{\partial x^2} - \lambda C + PS(x), \tag{2.16}$$

where D is the diffusion coefficient of the growth factor, λ the decay of the growth factor and P the production rate of the growth factor. These are all constants. $S(x)$ is the source term, describing the distribution of the growth factors, which is chosen to be piecewise uniform. So here $S(x) = 1$ at $L/2 \leq x \leq L/2 + \delta$ and $S(x) = 0$ elsewhere.

It is assumed that the distribution is independent of time, so $\dfrac{\partial C}{\partial t} = 0$. Furthermore the assumption has been made that the growth factors regulate the growth of bone. It is also presumed that there are no mechanical constraints, so the bone is free to grow into the wound.

Now the equation can be written as

$$\frac{d^2C}{dx^2} - \frac{\lambda}{D}C \;=\; -\frac{P}{D}, \qquad \frac{L}{2} \leq x \leq \frac{L}{2} + \delta, \tag{2.17}$$

$$\frac{d^2C}{dx^2} - \frac{\lambda}{D}C \;=\; 0, \qquad \text{elsewhere.} \tag{2.18}$$

Two models are investigated. In the first model it is assumed there is no tissue in the wound interior $-L/2 \leq x \leq L/2$, in the second model it is assumed that there is still some tissue in the wound interior.

The boundary conditions for model 1 are given by
(i) $C(x)$, $\frac{dC}{dx}$ are continuous at $x = L/2 + \delta$,
(ii)$\lim_{x\to\infty} C(x) = 0$,
(iii)$\frac{dC}{dx} = 0$ at $x = L/2$,

and the boundary condition for model 2 are given by
(i) $C(x)$, $\frac{dC}{dx}$ are continuous at $x = L/2$ and $x = L/2 + \delta$,
(ii)$\lim_{x\to\infty} C(x) = 0$,
(iii)$\frac{dC}{dx} = 0$ at $x = 0$.

Adam [9] presents some analytic solutions to the differential equations involved. A constitutive equation is used to describe the movement of the edge of the wound. When these models are solved, values for δ are obtained for which healing will occur.

Chapter 3

Numerical methods

The model to be solved in this paper will be the model due to Prendergast. To solve the differential equations numerical methods will be used. In this paper the Finite Element Method (FEM) will be used for discretisation in space and a semi-implicit method will be used for discretisation in time.

3.1 Space discretisation: FEM

First the weak formulations will be derived: The differential equations will be multiplied by an arbitrary, sufficiently smooth test function $\eta \in H^1(\Omega)$, with $\eta = 0$, where essential boundary conditions are given. After this the equations will be integrated.
First recall the equations

$$
\begin{aligned}
\frac{\partial c_m}{\partial t} &= \mathrm{div} D_m \nabla c_m + P_m(1 - c_{tot})c_m - F_f(1 - c_f)c_m \\
&\quad -F_c(1 - c_c)c_m - F_b(1 - c_b)c_m. \\
\frac{\partial c_f}{\partial t} &= \mathrm{div} D_f \nabla c_f + P_f(1 - c_{tot})c_f + F_f(1 - c_f)c_m - F_c(1 - c_c)c_f \\
&\quad -F_b(1 - c_b)c_f. \\
\frac{\partial c_c}{\partial t} &= P_c(1 - c_{tot})c_c + F_c(1 - c_c)(c_m + c_f) - F_b(1 - c_b)c_c, \\
\frac{\partial c_b}{\partial t} &= P_b(1 - c_{tot})c_b + F_b(1 - c_b)(c_m + c_f + c_c). \\
\frac{\partial m_f}{\partial t} &= Q_f(1 - m_{tot})c_f - (D_b c_b + D_c c_c)m_f m_{tot}, \\
\frac{\partial m_c}{\partial t} &= Q_c(1 - m_b - m_c)c_c - D_b c_b m_c m_{tot}, \\
\frac{\partial m_b}{\partial t} &= Q_b(1 - m_b)c_b.
\end{aligned}
$$

The FEM will be applied to equation (3.1). To show the procedure for the general case, the Robin boundary condition $D_m \frac{\partial c_m}{\partial n} = k_B(c_m - c_{mB})$ is used.

When $k_B \downarrow 0$ follows $D_m \dfrac{\partial c_m}{\partial n} = 0$, so a Neumann boundary condition is obtained.

If $k_B \to \infty$, then $c_m \to c_{mB}$ since c_m is smooth and it tends to a Dirichlet boundary condition.

Multiplying by η and integrating gives:

$$
\int_\Omega \eta \frac{\partial c_m}{\partial t} d\Omega \quad = \quad \int_\Omega \eta [D_m \text{div} \nabla c_m + P_m(1 - c_{tot})c_m \tag{3.1}
$$
$$
- F_f(1 - c_f)c_m - F_c(1 - c_c)c_m - F_b(1 - c_b)c_m] d\Omega.
$$

Writing out the terms yields

$$
\int_\Omega \eta \frac{\partial c_m}{\partial t} d\Omega \quad = \quad \int_\Omega D_m \eta \text{div} \nabla c_m d\Omega + \int_\Omega \eta Q c_m d\Omega, \tag{3.2}
$$

where $Q = P_m(1 - c_{tot}) - F_f(1 - c_f) - F_c(1 - c_c) - F_b(1 - c_b)$.

Integrating by parts the first term on the right-hand-side leaves

$$
\int_\Omega \eta \frac{\partial c_m}{\partial t} d\Omega = \int_\Gamma \eta D_m \frac{\partial c_m}{\partial n} d\Gamma - \int_\Omega \nabla \eta \cdot D_m \nabla c_m d\Omega + \int_\Omega \eta Q c_m d\Omega. \tag{3.3}
$$

The Robin boundary condition can be substituted to obtain

$$
\int_\Omega \eta \frac{\partial c_m}{\partial t} d\Omega \quad = \quad \int_\Gamma \eta k_B(c_m - c_{mB}) d\Gamma - \int_\Omega \nabla \eta \cdot D_m \nabla c_m d\Omega + \int_\Omega \eta Q c_m d\Omega
$$
$$
= \quad \int_\Gamma \eta k_B c_m d\Gamma - \int_\Gamma \eta k_B c_{mB} d\Gamma - \int_\Omega \nabla \eta D_m \nabla c_m d\Omega
$$
$$
+ \int_\Omega \eta Q c_m d\Omega, \tag{3.4}
$$

$\forall \eta \in H^1(\Omega)$.

This is the weak formulation, in which $c_m \in H^1(\Omega)$ is to be found.

Now the Galerkin equations can be derived. The solution is approximated by a linear combination of basis functions. Put

$$
c_m^n(\underline{x}) = \sum_{j=1}^n c_{m(j)}(t)\phi_j(\underline{x}), \tag{3.5}
$$

where $\phi_j(\underline{x}) \in H^1(\Omega)$ are the basis functions.

Since η is from the same space as c_m it is possible to write η as a linear combination of n basis functions

$$
\eta = \sum_{i=1}^n b_i \phi_i(\underline{x}). \tag{3.6}
$$

The function η is arbitrarily chosen, so for simplicity the coefficients of b_i are chosen equal to 1 and the others equal to 0. Then it follows that $\eta = \phi_i$ with $i = 1, ..., n$.

Substitution into the weak formulation (3.4) gives the Galerkin equations

$$
\begin{aligned}
\sum_{j=1}^{n} \int_{\Omega} \phi_i \phi_j \frac{dc_{m(j)}}{dt} d\Omega \;=\;& \sum_{j=1}^{n} c_{m(j)} \int_{\Gamma} \phi_i k_B \phi_j d\Gamma - \int_{\Gamma} \phi_i k_B c_{mB} d\Gamma \\
& - \sum_{j=1}^{n} c_{m(j)} \int_{\Omega} \nabla \phi_i D_m \nabla \phi_j d\Omega \qquad (3.7)\\
& + \sum_{j=1}^{n} c_{m(j)} \int_{\Omega} \phi_i Q \phi_j d\Omega.
\end{aligned}
$$

Since the FEM involves an element-by-element assembly of all the matrices and vectors for both internal and boundary elements, the development of the element matrices and vectors will now presented.

At first an integration rule will be given. This integration rule, called the Newton-Cotes rule, is based on the FEM basis function interpolation [10]:

$$
g(x) \approx \sum_{k=1}^{n+1} g(x_k) \phi_k(x). \qquad (3.8)
$$

Also the following theorem will be used [10]:

Theorem 3.1. *Let S_ε be a simplex in $\mathbb{R}^n$ and let $\triangle$ be the determinant defined by*

$$
\triangle = \begin{vmatrix}
1 & x_1^1 & x_2^1 & \cdots & x_n^1 \\
1 & x_1^2 & x_2^2 & \cdots & x_n^2 \\
\vdots & \vdots & \vdots & \vdots & \\
1 & x_1^{n+1} & x_2^{n+1} & \cdots & x_n^{n+1}
\end{vmatrix}, \qquad (3.9)
$$

with $\underline{x}^1$, $\underline{x}^2$, …, $\underline{x}^{n+1}$ the vertices of S_ε.
Let $\lambda_i(\underline{x})$ be the linear basis functions over S_ε defined by

$$
\begin{aligned}
& \lambda_i(\underline{x}) \;\; linear, \\
& \lambda_i(\underline{x}^j) = \delta_{ij}, \quad i,j = 1,2,\cdots,n+1. \qquad (3.10)
\end{aligned}
$$

Then the following general integral rule holds:

$$
\int_{S_\varepsilon} \lambda_1^{m_1} \lambda_2^{m_2} \cdots \lambda_{n+1}^{m_{n+1}} d\Omega = \frac{m_1! m_2! \cdots m_{n+1}!}{(\sum_i m_i + n)!} |\triangle|, \qquad (3.11)
$$

for all $m_i \geq 0$. $\qquad\qquad\qquad\qquad\qquad\qquad\qquad\qquad\qquad\qquad\qquad\qquad\square$

Triangular elements are chosen (see Figure 3.1), which use the function values at the three vertices of the triangle and a linear interpolation.
So for the basis functions the following holds:

$$
\begin{aligned}
& \phi_i(\underline{x}) = \underline{a}_0^i + \underline{a}_1^i x + \underline{a}_2^i y, \\
& \phi_i(\underline{x}^j) = \delta_{ij}, \quad i,j = 1,2,\cdots,n+1, \qquad (3.12)
\end{aligned}
$$
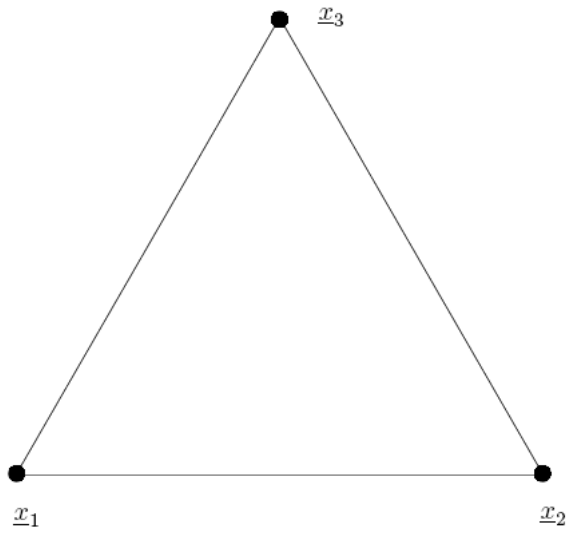
Figure 3.1: Linear triangular element, for the interior points, where $|\triangle|$ is equal to two times the area of the triangle.

Figure 3.2: Linear line element, for the boundary points, where S_{ε} is the length of the line.

The Newton-Cotes rule for these triangles ($n = 2$) for interior points is given by

$$
\begin{aligned}
\int_{S_\varepsilon} g(\underline{x})d\Omega &= \int_{S_\varepsilon} \sum_{k=1}^{n+1} g(\underline{x}_k)\phi_k(\underline{x})d\Omega \\
&= \sum_{k=1}^{n+1} g(\underline{x}_k) \int_{S_\varepsilon} \phi_k(\underline{x})d\Omega \\
&= \sum_{k=1}^{n+1} g(\underline{x}_k) \frac{1!}{(1+2)!}|\triangle| \\
&= \frac{|\triangle|}{6}(g(\underline{x}_1) + g(\underline{x}_2) + g(\underline{x}_3)).
\end{aligned} \tag{3.13}
$$

For points on the boundary the simplex is a line ($n = 1$, see Figure 3.2) and so the Newton-Cotes rules is given by

$$
\begin{aligned}
\int_{S_\varepsilon} h(\underline{x})d\Omega &= \sum_{k=1}^{n+1} g(\underline{x}_k) \frac{1!}{(1+1)!}|\triangle| \\
&= \frac{\ell(S_\varepsilon)}{2}(g(\underline{x}_1) + g(\underline{x}_2)).
\end{aligned} \tag{3.14}
$$

Note that this is the trapezoidal rule.

Using this the integrals from (3.8) can be solved.
For the integral on the left hand side it follows:

$$
\begin{aligned}
\int_\Omega \phi_i\phi_j d\Omega &= \frac{|\triangle|}{6} \sum_{k=1}^{3} \phi_i(\underline{x}_k)\phi_j(\underline{x}_k) \\
&= \frac{|\triangle|}{6}\delta_{ij},
\end{aligned} \tag{3.15}
$$

$$
\tag{3.16}
$$

where δ_{ij} is the Kronecker delta.
This will be entered in the Mass-time-matrix M_{time}, so

$$
M_{time}^{el} = \frac{|\triangle|}{6} \begin{bmatrix} 1 & 0 & 0 \\ 0 & 1 & 0 \\ 0 & 0 & 1 \end{bmatrix}.
$$

From the first integral on the right hand side it follows

$$
\begin{aligned}
\int_\Gamma \phi_i k_B \phi_j d\Gamma &= \frac{\ell(S_\varepsilon)}{2} \sum_{k=1}^{2} \phi_i(\underline{x}_k)k_B\phi_j(\underline{x}_k) \\
&= \frac{\ell(S_\varepsilon)}{2}k_B\delta_{ij},
\end{aligned} \tag{3.17}
$$

which will be added to the Mass-matrix R, so

$$
R^{el} = -\frac{|\triangle|}{2}k_B \begin{bmatrix} 1 & 0 \\ 0 & 1 \end{bmatrix}.
$$

The second integral on the right hand side leads to

$$-\int_\Gamma \phi_i k_B c_{mB} d\Gamma \quad = \quad -\frac{\ell(S_\varepsilon)}{2} \sum_{k=1}^{2} \phi_i(x_k) k_B c_{mB} d\Gamma$$

$$= \quad -\frac{\ell(S_\varepsilon)}{2} k_B c_{mB}, \tag{3.18}$$

contained in the element vector f:

$$f^{el} = -\frac{\ell(S_\varepsilon)}{2} k_B c_{mB} \begin{bmatrix} 1 \\ 1 \end{bmatrix}.$$

The third integral contributes to the stiffness-matrix Z

$$-\int_\Omega \nabla\phi_i D_m \nabla\phi_j d\Omega \quad = \quad -\frac{|\triangle|}{6}(a_1^i a_1^j + a_2^i a_2^j) \sum_{k=1}^{3} D_m(\underline{x}_k),$$

so

$$Z^{el} = \frac{|\triangle|}{6} \sum_{k=1}^{3} D_m(\underline{x}_k) \begin{bmatrix} (a_1^1 a_1^1 + a_2^1 a_2^1) & (a_1^1 a_1^2 + a_2^1 a_2^2) & (a_1^1 a_1^3 + a_2^1 a_2^3) \\ (a_1^2 a_1^1 + a_2^2 a_2^1) & (a_1^2 a_1^2 + a_2^2 a_2^2) & (a_1^2 a_1^3 + a_2^2 a_2^3) \\ (a_1^3 a_1^1 + a_2^3 a_2^1) & (a_1^3 a_1^2 + a_2^3 a_2^2) & (a_1^3 a_1^3 + a_2^3 a_2^3) \end{bmatrix}.$$

The last integral is contained in the mass-matrix R:

$$\int_\Omega \phi_i Q \phi_j d\Omega \quad = \quad \frac{|\triangle|}{6} \sum_{k=1}^{3} \phi_i(\underline{x}_k) Q(\underline{x}_k) \phi_j(\underline{x}_k)$$

$$= \quad \frac{|\triangle|}{6} Q(\underline{x}_i) \delta_{ij}, \tag{3.19}$$

so the element matrix looks like

$$R^{el} = -\frac{|\triangle|}{6} \begin{bmatrix} Q(\underline{x}_1) & 0 & 0 \\ 0 & Q(\underline{x}_2) & 0 \\ 0 & 0 & Q(\underline{x}_3) \end{bmatrix}.$$

So at the end the equation for (3.1) becomes

$$M_{time} \frac{d\underline{c}_m}{dt} = (-Z - R)\underline{c}_m + \underline{f}, \tag{3.20}$$

where Z the stiffness matrix follows from the diffusion term and R is the mass matrix following from the reaction term. M_{time} is the time mass matrix.

3.2   Time discretisation: Semi-implicit method

Recall equation 3.20. Since R also contains a term with c_m this is a non-linear equation.
This term should be linearized and to that purpose there are three methods [11]:

(i)   Newton: $(c_{m(j)}^{n+1})^2 \simeq 2c_{m(j)}^{n+1} c_{m(j)}^{n} - (c_{m(j)}^{n})^2,$

(ii)   Picard:$(c_{m(j)}^{n+1})^2 \simeq c_{m(j)}^{n+1} c_{m(j)}^n$,

(iii)   extrapolated Picard: $(c_{m(j)}^{n+1})^2 \simeq (2c_{m(j)}^n - c_{m(j)}^{n-1})(c_{m(j)}^{n+1})^2.$

In this report Picard linearization will be chosen. Choosing to use the values of c_m on the future time step and the other values at the present, time-discretisation looks as follows (dropping underlines):

$$M_{time} \frac{c_m^{n+1} - c_m^n}{\tau} = (-Z^n - R^n)c_m^{n+1} + f^n. \tag{3.21}$$

So

$$(\frac{M_{time}}{\tau} + Z^n + R^n)c_m^{n+1} = \frac{M_{time}}{\tau}c_m^n + f^n. \tag{3.22}$$

Chapter 4

Results for the model due to Prendergast

In this chapter the stimulus is kept constant and the biological part of the model is investigated. Keeping a constant mechanical stimuli of $S = 1$, the values for the fibroblast concentrations c_f and the fibrous matrix m_f are 0. The following values for the parameters are used:

$D_{m0} = 2.37$, $D_{f0} = 0.1152$, $P_{m0} = 1.2$, $P_{f0} = 0.1$, $P_{c0} = 0.75$, $P_{b0} = 0.5$, $F_f = 0.01$, $F_c = 0.3$, $F_b = 0.15$, $Q_f = 0.06$, $Q_c = 0.2$, $Q_b = 0.1$, $D_c = 0.2$, $D_b = 0.1$.

The prosthesis, see figure 4.1, is assumed to be 10 mm thick in total. The upper layer (Ω_1), chosen to be 5 mm thick, consists of polyethylene, where bone cannot grow into. The lower layer, chosen to be 5 mm thick also, consists of porous tantalum, and this is the region where the bone grows into. For this simulation only the area Ω_2 is considered.

It is shown in figure 4.2 that after 80 days the concentration of mesenchymal cells is zero, except for the Dirichlet boundary. Near the same boundary the concentration of the chondrocytes, see Figure 4.3, is high and gets lower towards the end of the prosthesis.

For the osteoblasts density the same holds as for the chondrocyte density: The highest value can be seen at the implant-bone interface and decreases towards the end of the prosthesis.
As said before, the concentrations of the fibroblasts and of the fibrous tissue are zero.

Endochondral ossification has started and the matrix density of the cartilage is fading, see Figure 4.5. The highest value 0.115 is seen at the implant-shoulder interface. The bone matrix density already increased, with the highest value 0.905 in the end of the prosthesis, see Figure 4.6.

In Figure 4.7 the different values of the cell- and matrix concentrations through time are shown, for a point in the middle of the prosthesis. The red line represents the mesenchymal cellular density, the cyan line shows the chondrocyte
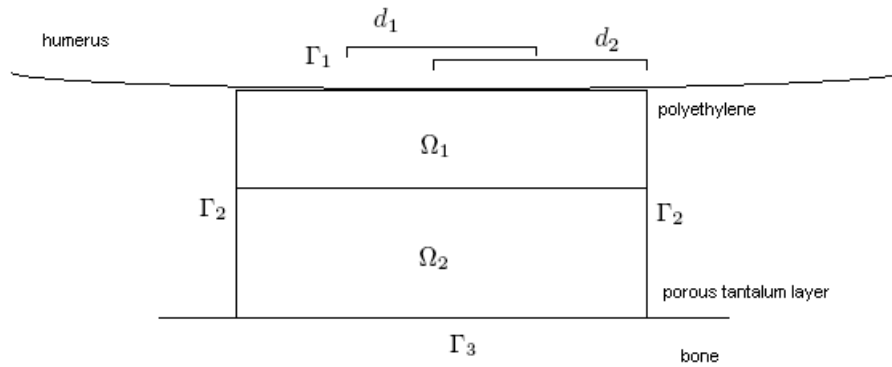
Figure 4.1: The geometry of the Bone-Implant interface.
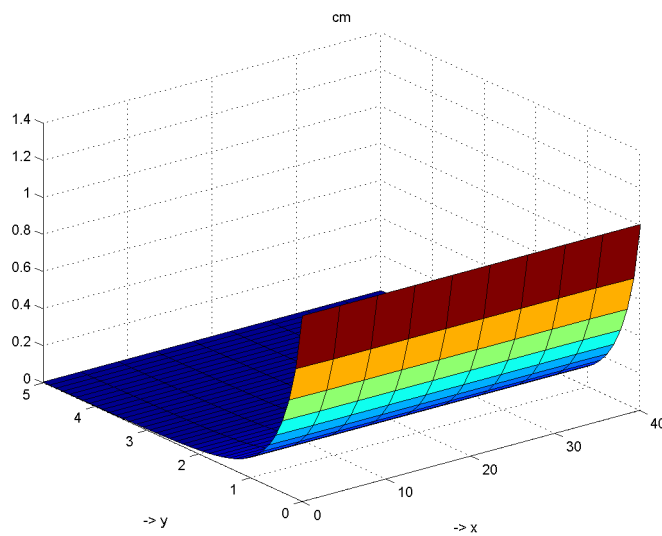
Figure 4.2: The concentration of the mesenchymal cells at $T = 80$, while stimulus S is kept at a value of 1.

concentration and the green line is the osteoblast density. The dotted lines stand for the matrix densities, the cyan one representing cartilage and the green one representing bone.

So if the stimulus is kept at a value of 1, the endochondral ossification process start around day 30. From that moment on the cartilage density starts to decrease.
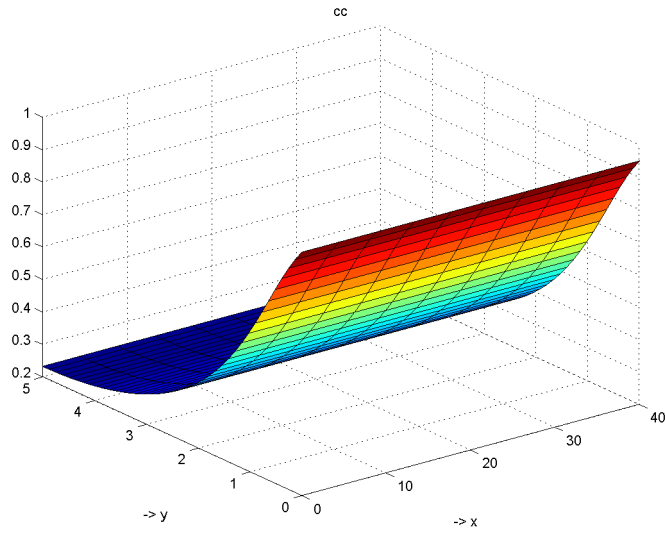
Figure 4.3: The concentration of the chondrocytes at $T = 80$, while stimulus S is kept at a value of 1.
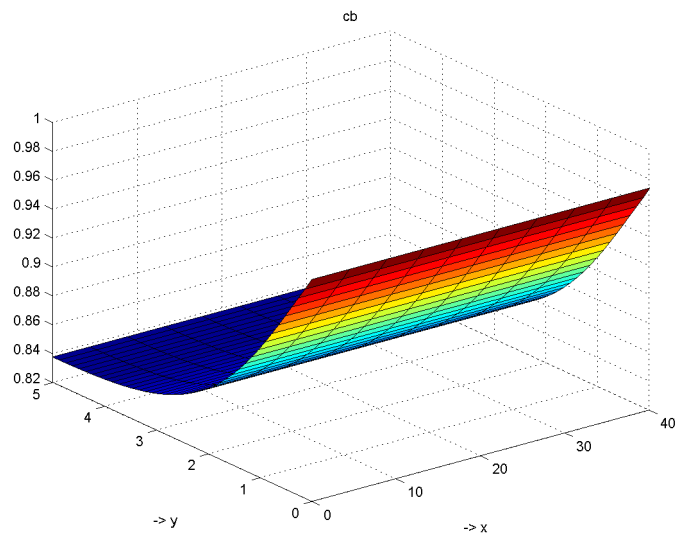
Figure 4.4: The concentration of the osteoblasts at $T = 80$, while stimulus S is kept at a value of 1.
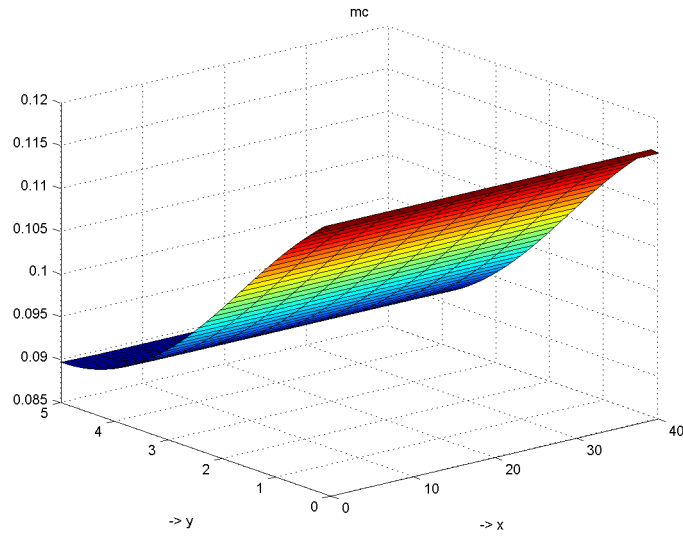
Figure 4.5: Cartilage matrix at $T = 80$, while stimulus S is kept at a value of 1.
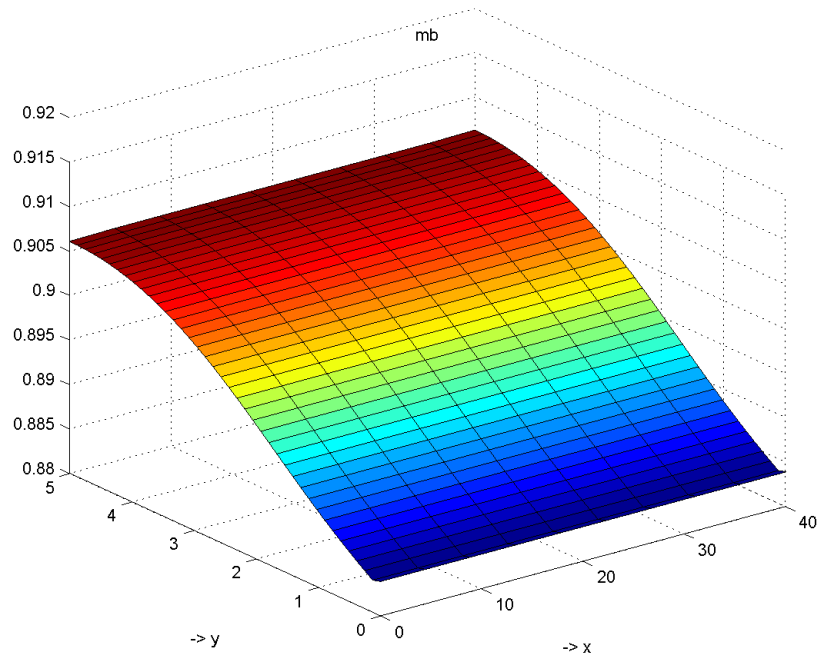
Figure 4.6: Bone matrix at $T = 80$, while stimulus S is kept at a value of 1.
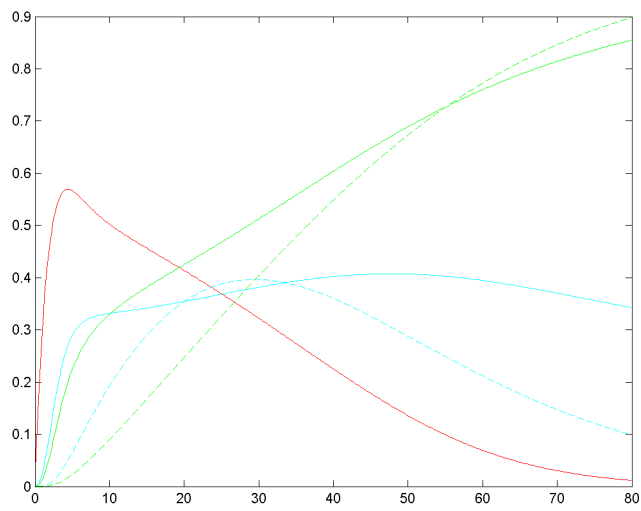
Figure 4.7: The cell and matrix densities, keeping stimulus S at 1, $T = 80$, at point $n/2$.

Chapter 5

FEM for the model due to Bailon-Plaza

Also to the model due to Bailon-Plaza the FEM will be applied. This will be shown only for the first equation. Recall the first equation:

$$\frac{\partial c_m}{\partial t} + \nabla \cdot (Cc_m\nabla m) = \text{div}(D\nabla c_m) + [A_m(1 - \alpha_m c_m) - F1 - F2]c_m.$$

The weak formulation is derived by multiplying with test function η and integrate over Ω. This leads to

$$\int_\Omega \eta\frac{\partial c_m}{\partial t}d\Omega + \int_\Omega \eta\nabla \cdot (Cc_m\nabla m)d\Omega = \int_\Omega \eta\nabla \cdot (D\nabla c_m)d\Omega + \int_\Omega \eta Qc_m d\Omega,$$

where $Q = A_m(1 - \alpha_m c_m) - F_1 - F_2$, taken at the previous time step. Integrating the second and third integral by parts, leads to

$$\int_\Omega \eta\frac{\partial c_m}{\partial t}d\Omega + \int_\Gamma \eta Cc_m\frac{\partial m}{\partial n}d\Gamma - \int_\Omega \nabla\eta \cdot Cc_m\nabla m d\Omega = \int_\Gamma \eta D\frac{\partial c_m}{\partial n}d\Gamma$$
$$- \int_\Omega \nabla\eta \cdot D\nabla c_m d\Omega + \int_\Omega \eta Qc_m d\Omega.$$

Applying the Dirichlet and Neumann boundary conditions leaves

$$\int_\Omega \eta\frac{\partial c_m}{\partial t}d\Omega - \int_\Omega \nabla\eta \cdot Cc_m\nabla m d\Omega = - \int_\Omega \nabla\eta \cdot D\nabla c_m d\Omega + \int_\Omega \eta Qc_m d\Omega. \quad (5.1)$$

Next, the Galerkin equations can be derived, by setting $\eta = \phi_i(\underline{x})$ and

$$c_m^n(\underline{x}) = \sum_{j=1}^n c_{m(j)}(t)\phi_j(\underline{x}),$$

and

$$m^n(\underline{x}) = \sum_{j=1}^n m_j(t)\phi_j(\underline{x}).$$

At the end c_m is the unknown to be solved for this equation, for m_j the values at the previous time step will be used.

Adding this to equation (5.1), it follows:

$$\sum_{j=1}^{n} \frac{dc_{m(j)}}{dt} \int_{\Omega} \phi_i \phi_j - \sum_{j=1}^{n} c_{m(j)} m_j (a_1^i a_1^j + a_2^i a_2^j) \int_{\Omega} C\phi_j d\Omega =$$

$$-\sum_{j=1}^{n} c_{m(j)} (a_1^i a_1^j + a_2^i a_2^j) \int_{\Omega} D d\Omega + \sum_{j=1}^{n} c_{m(j)} \int_{\Omega} \phi_i Q \phi_j d\Omega. \quad (5.2)$$

The integrals are computed by applying the Newton cotes rule. Recall

$$\int_{\Omega} \phi_i \phi_j d\Omega = \frac{|\triangle|}{6} \delta_{ij},$$

with δ_{ij} the Kronecker delta, and

$$\int_{\Omega} \phi_i Q \phi_j d\Omega = \frac{|\triangle|}{6} Q(\underline{x}_i) \delta_{ij}.$$

The corresponding element matrices are given by

$$M_{time}^{el} = \frac{|\triangle|}{6} \begin{bmatrix} 1 & 0 & 0 \\ 0 & 1 & 0 \\ 0 & 0 & 1 \end{bmatrix},$$

and

$$R^{el} = \frac{|\triangle|}{6} \begin{bmatrix} Q(\underline{x}_1) & 0 & 0 \\ 0 & Q(\underline{x}_2) & 0 \\ 0 & 0 & Q(\underline{x}_3) \end{bmatrix}.$$

For the second integral on the left-hand-side of (5.2) it follows

$$\int_{\Omega} C\phi_j d\Omega = \frac{|\triangle|}{6} C(\underline{x}_j)$$

and the element matrix is represented by

$$Y^{el} = \frac{|\triangle|}{6} \begin{bmatrix} Y_{11} & Y_{12} & Y_{13} \\ Y_{21} & Y_{22} & Y_{23} \\ Y_{31} & Y_{32} & Y_{33} \end{bmatrix},$$

where $Y_{ij} = (a_1^i a_1^j + a_2^i a_2^j) m(\underline{x}_j) C(\underline{x}_j)$.

For the first integral on the right-hand-side of (5.2) it follows

$$\int_{\Omega} D d\Omega = \frac{|\triangle|}{6} \sum_{k=1}^{3} D(\underline{x}_k),$$

with element matrix

$$Z^{el} = \frac{|\triangle|}{6} \sum_{k=1}^{3} D(\underline{x}_k) \begin{bmatrix} (a_1^1 a_1^1 + a_2^1 a_2^1) & (a_1^1 a_1^2 + a_2^1 a_2^2) & (a_1^1 a_1^3 + a_2^1 a_2^3) \\ (a_1^2 a_1^1 + a_2^2 a_2^1) & (a_1^2 a_1^2 + a_2^2 a_2^2) & (a_1^2 a_1^3 + a_2^2 a_2^3) \\ (a_1^3 a_1^1 + a_2^3 a_2^1) & (a_1^3 a_1^2 + a_2^3 a_2^2) & (a_1^3 a_1^3 + a_2^3 a_2^3) \end{bmatrix}.$$

At the end the equation to be solved is:

$$M_{time} \frac{d\underline{c}_m}{dt} = (-Y - Z - R)\underline{c}_m + \underline{f},$$

where Z the stiffnessmatrix, following from the diffusion term. Matrix Y comes from the convection term and R is the mass matrix following from the reaction term. M_{time} is the time mass matrix.

For discretisation in time the semi-implicit scheme from Section 3.2 is used again. Then the following system is obtained

$$\left[\frac{M_{time}}{\tau} + Y^n + Z^n + R^n \right] c_m^{n+1} = \left(\frac{M_{time}}{\tau} \right) c_m^n + f^n.$$

Chapter 6

Results Bailon-Plaza

The following values for the parameters are used:

$\alpha_m = 1$, $\alpha_c = 1$, $\alpha_b = 1$, $A_{m0} = 1.01$, $A_{c0} = 1.01$, $A_{b0} = 0.202$, $P_{cs} = 0.2$, $P_{bs} = 2$, $H_1 = 0.1$, $H_2 = 0.1$, $H_3 = 0.1$, $\kappa_b = 1$, $\kappa_c = 1$, $D_h = 0.014$, $C_k = 0.0034$, $K_h = 0.25$, $K_k = 0.5$, $K_b = 0.1$, $K_m = 0.1$, $K_c = 0.l$, $D_{gc} = 0.005$, $D_{gb} = 0.005$, $Y_1 = 10$, $Y_2 = 50$, $Y_3 = 100$, $Q_{cd} = 2$, $B_{ec} = 1.5$, $d_b = 0.1$, $G_{gc} = 50$, $G_{gb} = 500$, $H_{gc} = 1$, $H_{gb} = 1$, $K_{gc} = 0.1$, $d_{gc} = 100$, $d_{gb} = 100$.

The simulation takes place on a 1×1.3 rectangular grid, where the growth factors of bone originate from $\{y \in (0, 0.5), x = 0\}$, which represents the bone. This is the blue line in Figure 6.1. The cartilage growth factors originate from the fracture gap which will be placed at $\{x \in (0, 0.3), y = 1.3\}$ (the green line). The mesenchymal cells originate from the periosteum and the surrounding tissue, which will be placed at $(y = 0, x > 0.5) \cap (x = 1, y < 0.65)$ (the black line). The reason for this is that the mesenchymal cells and bone growth factors originate from surfaces very close to each other (the bone and the periosteum), while the fracture gap, where the cartilage growth factors originate from, lies more far away.

As can be seen from Figure 6.2 the mesenchymal cells originate from the broken periosteum and the chondrocytes originate from the fracture gap into the callus. Along the bone the osteoblasts are spreading.

6.1   Fracture healing after 2.4 days

The concentration of cartilage, which was 0.1 at the beginning, has increased under influence of the mesenchymal cells and the chondrocytes, and the cartilage growth factors have spread into the callus (see Figure 6.3). The bone growth factors are also diffusing towards the callus and already some bone has been appeared under influence of the osteoblasts.
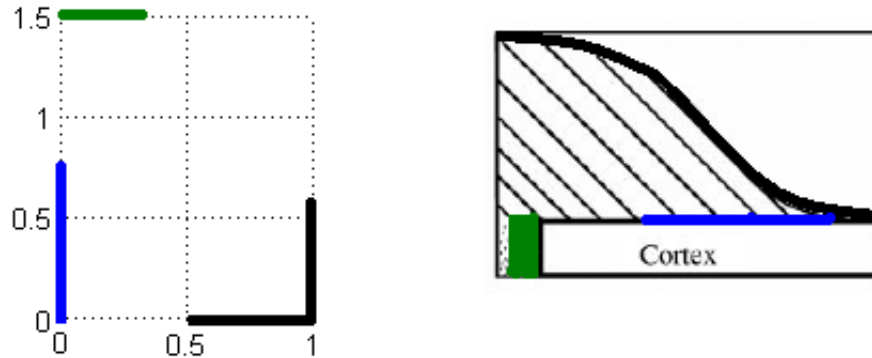
Figure 6.1: Geometry of the callus. Left: the grid used in the simulation. Right: the actual geometry of the fracture. The green line represents the surface where the cartilage growth factor originate from, the blue line represents the bone growth factors and the black line represents the source of mesenchymal cells.
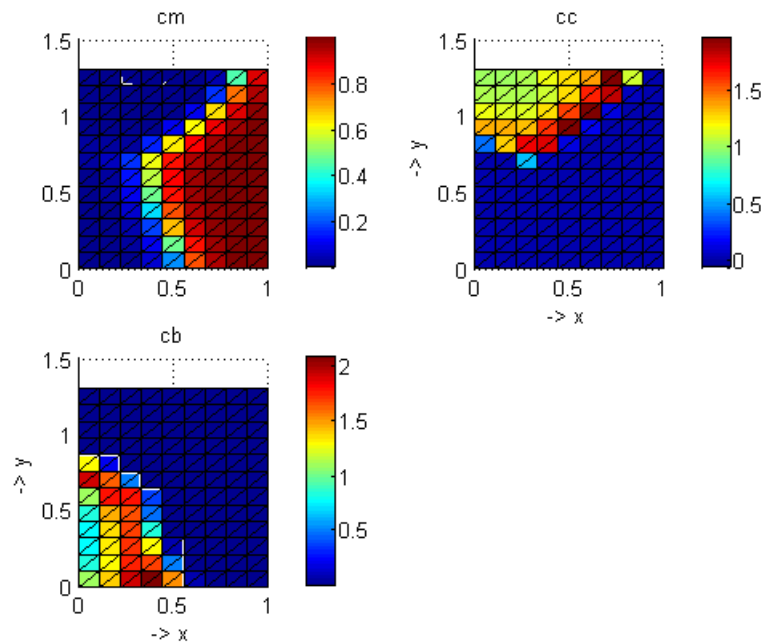
Figure 6.2: Mesenchymal cell (upper left picture), chondrocyte (upper right picture) and osteoblasts (lower left picture) density after 2.4 days.

6.2   Fracture healing after 4 days

After 4 days concentration of the mesenchymal cells has decreased and only remains at a high level near the periosteum. The concentrations of chondrocytes
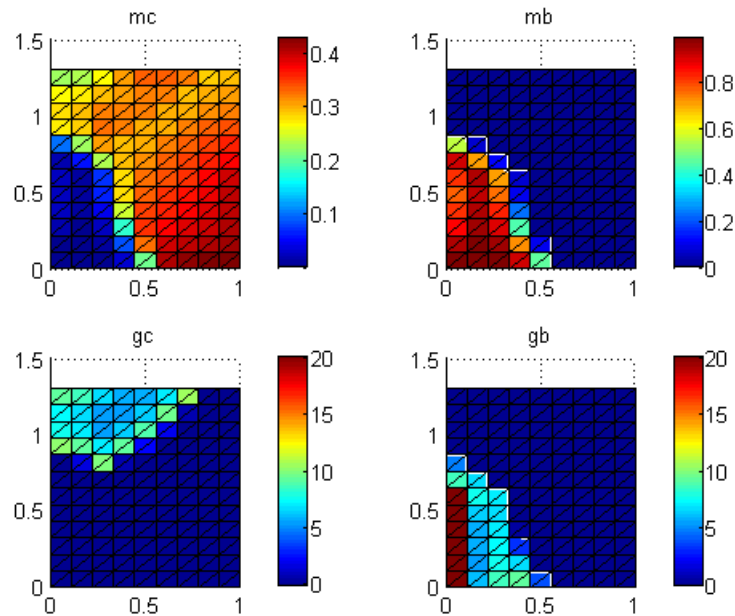
Figure 6.3: Cartilage (upper left picture) and bone matrix (upper right picture) density and concentration of growth factors of cartilage (lower left picture) and bone (lower left picture), after 2.4 days.

and osteoblasts both have increased and spread out, see Figure 6.4.

The cartilage and bone matrix has both increased and approach each other in the callus. The cartilage growth factor has decreased to a value of 2, while the bone growth factors cover a larger area now, see Figure 6.5.

6.3   Fracture healing after 8 days

After 8 days the mesenchymal cells have almost disappeared, while the chondrocyte concentration has increased to 1 at certain areas. The osteoblasts front is moving throughout the whole area now, see Figure 6.6.

Cartilage is slowly getting 'pushed back' by bone and the cartilage growth factors are also disappearing. The growth factors of bone has also decreased to a value around 3, see Figure 6.7.

6.4   Fracture healing after 20 days

After 20 days the concentration of chondrocytes is 1 throughout almost the whole callus and the osteoblasts concentration has a value around 0.55 almost everywhere, see Figure 6.8.
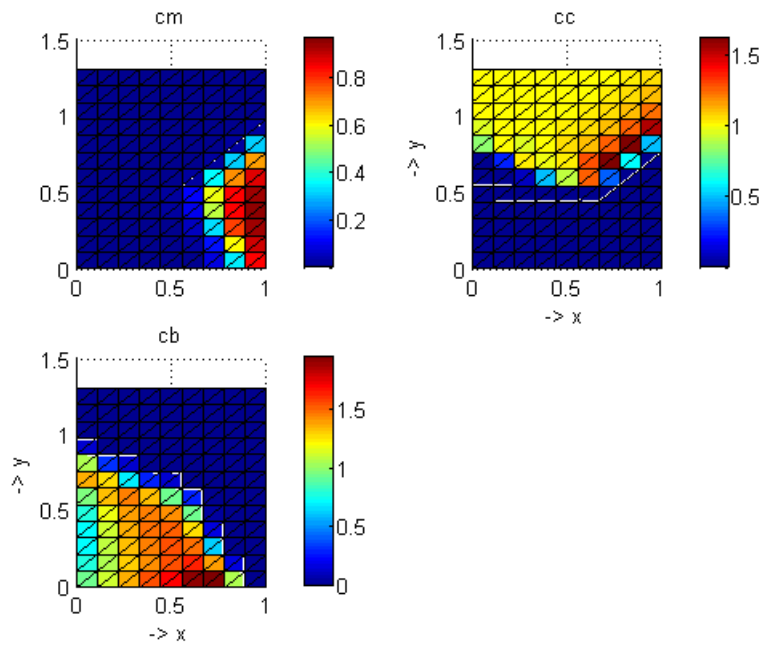
Figure 6.4: Mesenchymal cell (upper left picture), chondrocyte (upper right picture) and osteoblasts (lower left picture) density after 4 days.

In Figure 6.9 the cell densities at a certain point X in the area are shown as a function of time. The mesenchymal cell front has reached this point around day 2, whereafter the chondrocytes peak at day 3. After day 3 the osteoblast density grows to a value of 0.5 and after that slowly decreases. The whole callus is filled with bone now, and there is also a small concentration of 0.15 cartilage present. The growth factor concentrations of cartilage is zero now while the growth factors of bone decreased to a level around 2, see Figure 6.10.

Figure 6.11 shows the matrix densities of point X as a function of time. The cartilage starts at a value of 0.1 and increases to a value of 0.5 around day 4. After that the endochondral ossification starts and the value of cartilage will decrease and bone will appear. The cartilage growth factor peaks at day 3 and the bone growth factors reach this point around day 5.

6.5   Important parameters

It is interesting to analyze the influence of the different parameters. An increase of A_{b0} to a value of 1.01 leads after 20 days to an higher value of the osteoblast density. The chondrocyte density at day 20 is the same, but the peak around day 3 is lower. Cartilage has appeared in the same area but the density is lower, and now stays at a value of 0.1, while bone seems to grow faster. The bone growth factor concentration has increased to a value around 3.5 throughout the whole callus. Figure 6.12 shows the densities at point X as a function of time.
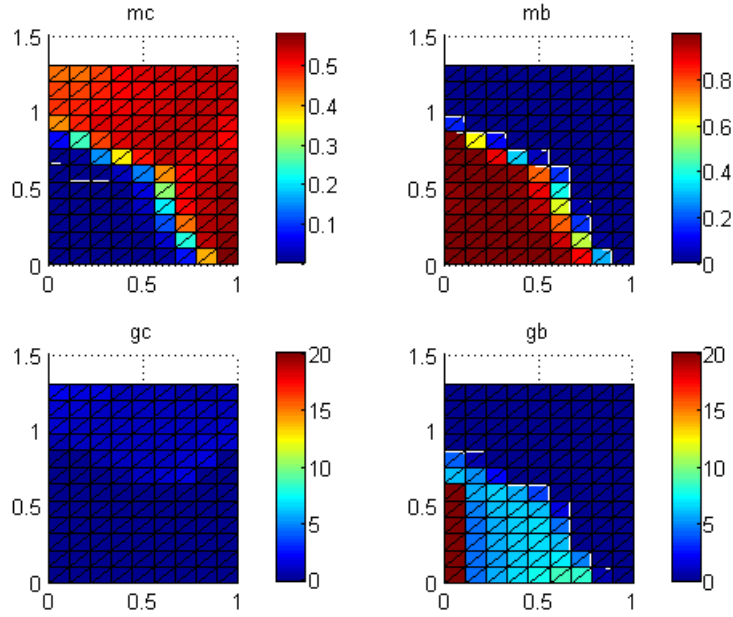
Figure 6.5: Cartilage (upper left picture) and bone matrix (upper right picture) density and concentration of growth factors of cartilage (lower left picture) and bone (lower left picture), after 4 days.

Taken the value of F_1 twice as high, seems to have no influence on the mesenchymal cell density . The peak of the chondrocyte density at day 3 is lower. Less cartilage has been created and also the cartilage growth factor has a lower peak. The growth of bone seems to start a little earlier.

Doubling the value of F_3 does not have much influence. The growth of bone proceeds a little faster, but makes no significant difference.

An increase of the value d_{gb} to 150, leads to a slower healing process, see Figure 6.13. More cartilage will appear and the growth of bone starts a few days later. Also the bone growth factor concentrations remains longer at a zero value. Increasing E_{gb} leads to a very high value of bone growth factor, which is not very surprising, and a very fast healing.

Doubling the value of D_{gc} shows, of course, a higher concentration of cartilage growth factors and a little higher density of cartilage. However, it has very little influence on the production of bone or the bone growth factors. The same holds for doubling E_{gc}.

A big influence seems to be the bone production rate P_{bs}, see Figure 6.14. For a lower value of P_{bs} the bone growth process takes a lot longer.
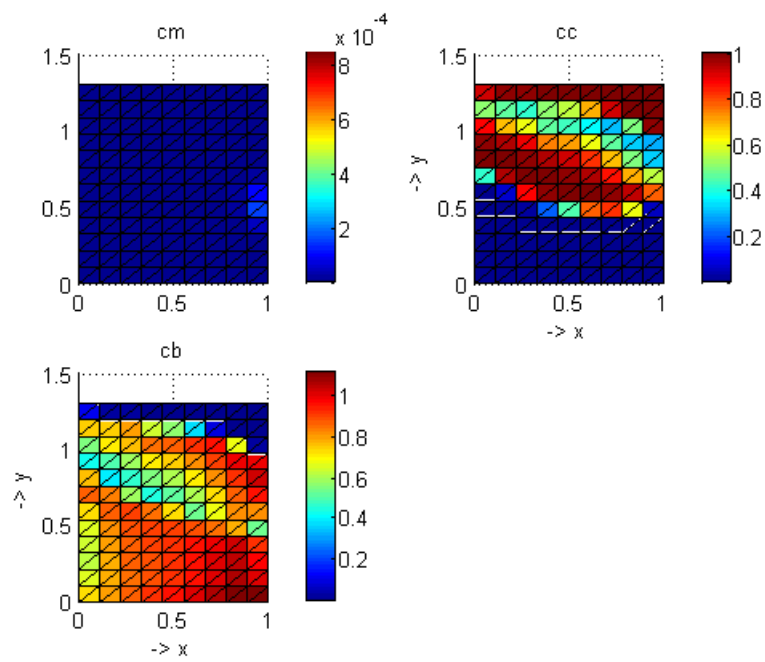
Figure 6.6: Mesenchymal cell (upper left picture), chondrocyte (upper right picture) and osteoblasts (lower left picture) density after 8 days.
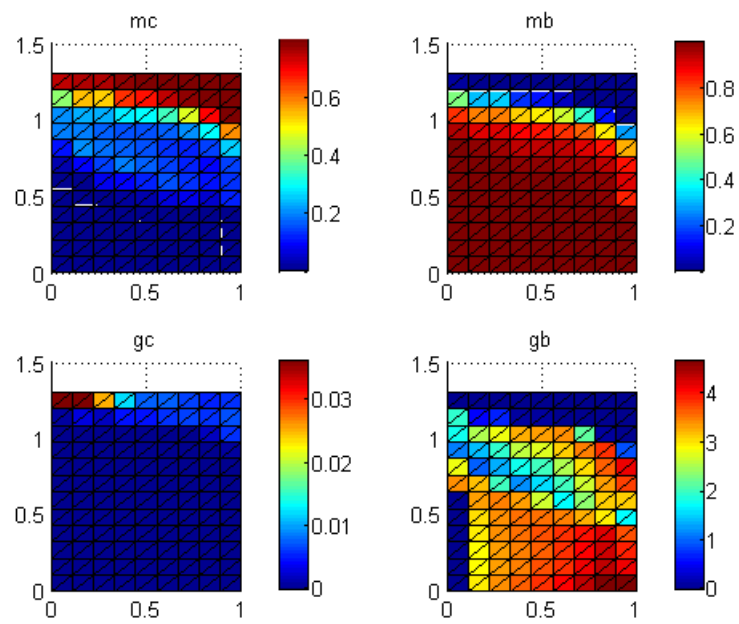
Figure 6.7: Cartilage (upper left picture) and bone matrix (upper right picture) density and concentration of growth factors of cartilage (lower left picture) and bone (lower left picture), after 8 days.
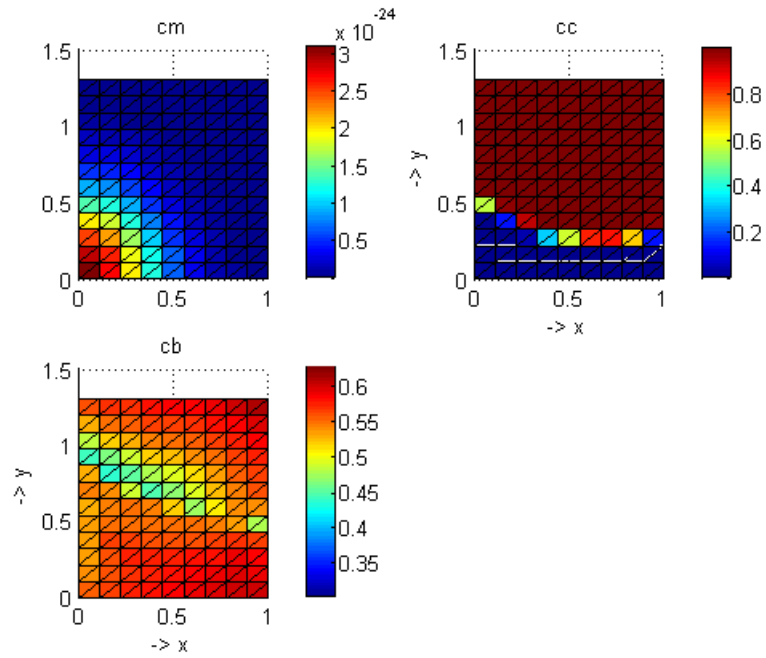
Figure 6.8: Mesenchymal cell (upper left picture), chondrocyte (upper right picture) and osteoblasts (lower left picture) density after 20 days.
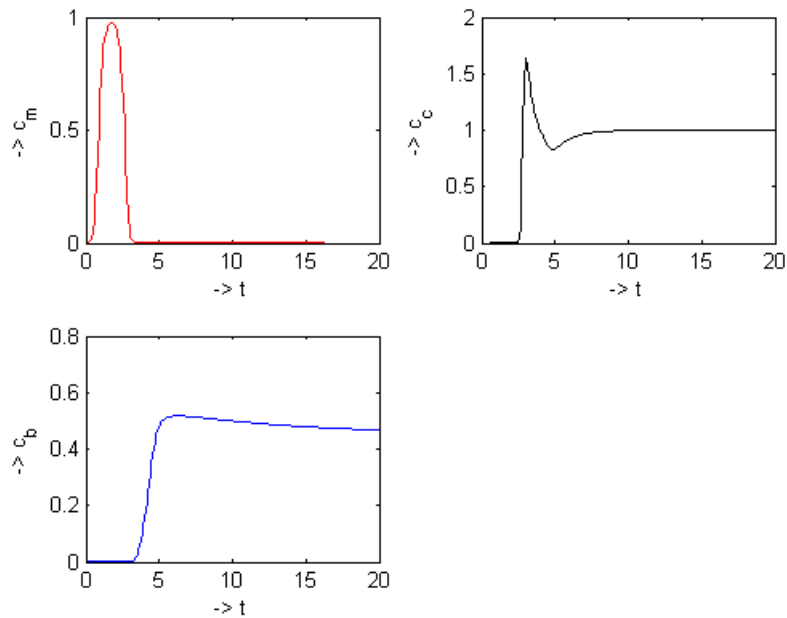
Figure 6.9: Mesenchymal cell (upper left), chondrocyte (upper right) and osteoblasts density (lower left) after 20 days.
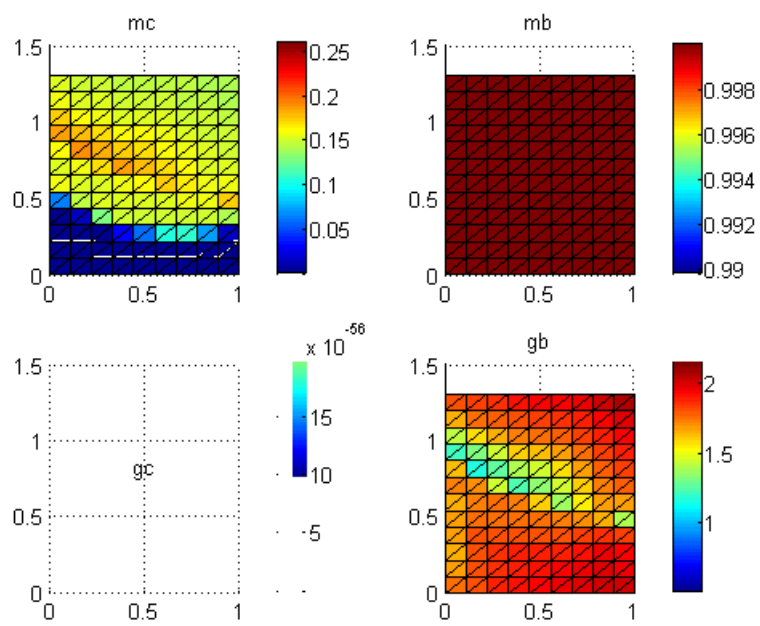
Figure 6.10: Cartilage (upper left picture) and bone matrix (upper right picture) density and concentration of growth factors of cartilage (lower left picture) and bone (lower left picture), after 20 days
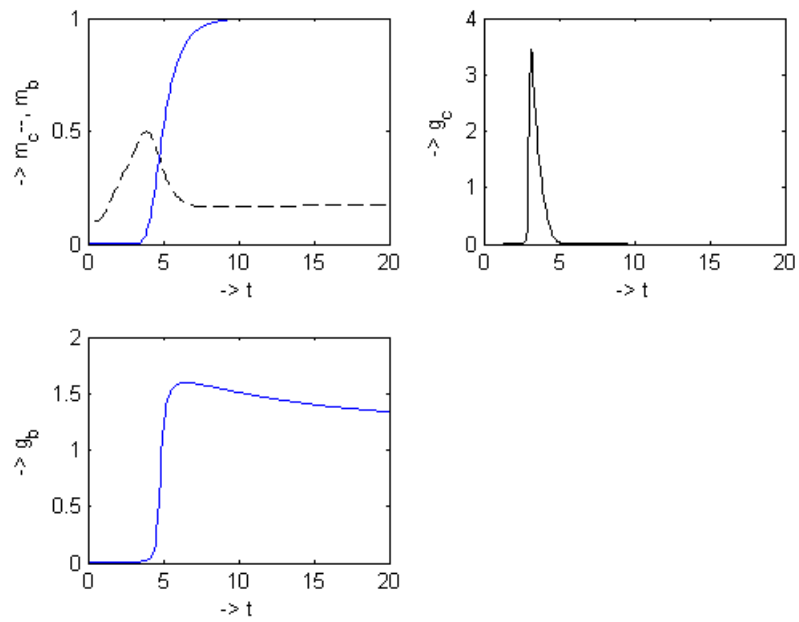
Figure 6.11: Cartilage (- - - -)and bone(——) densities (upper left picture) and their growth factors (upper right: cartilage growth factor, lower left: bone growth factor), as a function of time.
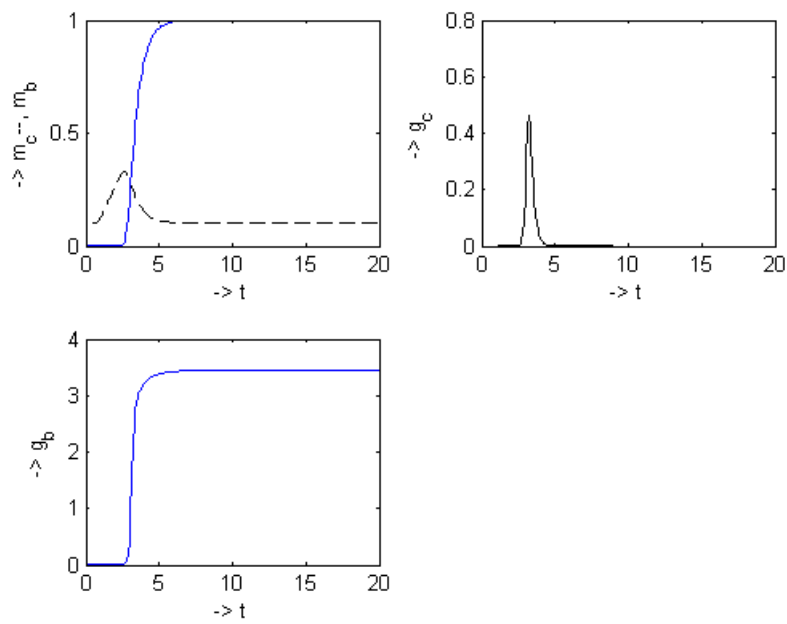
Figure 6.12: The value of A_{b0} has been set at 1.01. Cartilage (- - - -)and bone(—–) densities (upper left picture) and their growth factors (upper right: cartilage growth factor, lower left: bone growth factor), as a function of time. The cartilage density is lower, while bone growth proceeds faster.
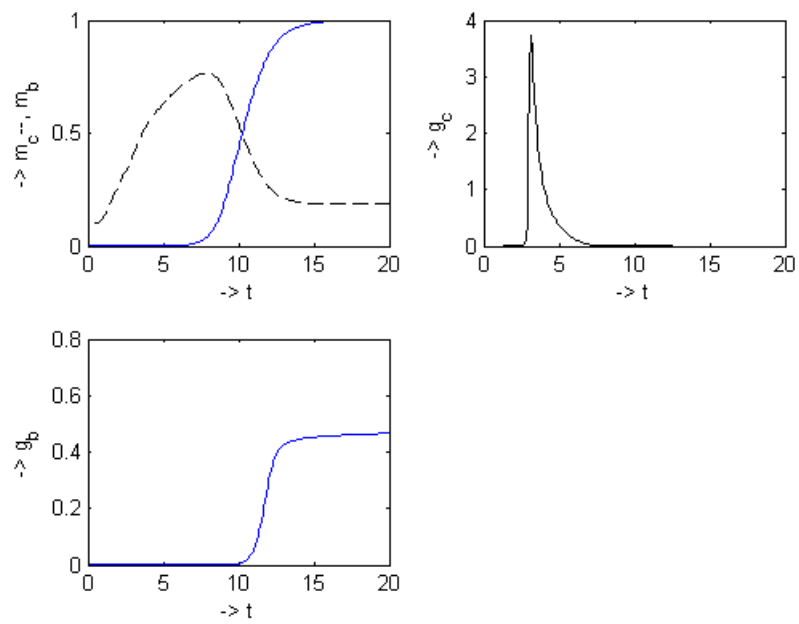
Figure 6.13: For a higher value of d_{gb}. Cartilage (- - - -)and bone(——) densities (upper left picture) and their growth factors (upper right: cartilage growth factor, lower left: bone growth factor), as a function of time. More cartilage has appeared, while it takes longer for bone to grow in.
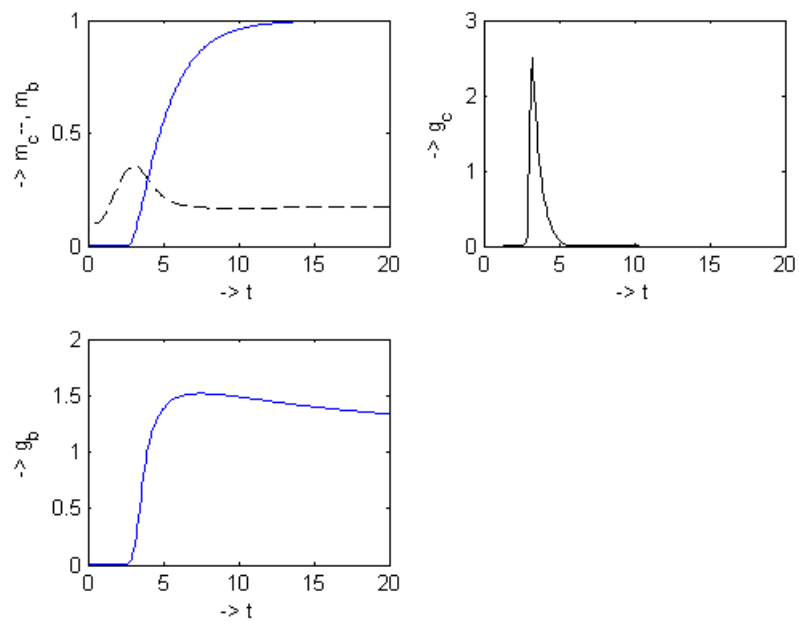
Figure 6.14: For a higher value of P_{bs}. Cartilage (- - - -)and bone(——) densities (upper left picture) and their growth factors (upper right: cartilage growth factor, lower left: bone growth factor), as a function of time. It takes longer before the bone has fully grown in.

Chapter 7

The poro-elastic model

As mentioned in Section 2.1, the proliferation and differentiation rates of the cells depend on the mechanical stimulus S. The stimulus S is defined by

$$S = \frac{\gamma}{a} + \frac{\nu}{b}, \tag{7.1}$$

with $a = 0.0375$ and $b = 3\mu m/s$, γ being the maximum shear strain and ν the relative fluid/solid velocity. The shear strain is a measure of the mechanical stimulus in the solid and the fluid velocity is a measure of the agitation in the precursor cell pool [12].
Bone will develop if $S < 1$, cartilage if $1 < S < 3$ and fibrous tissue for $S > 3$, see Appendix A.

From the poro elastic model values for u,v and p are obtained. In 2-D the Cauchy strain tensor is defined as

$$\underline{\underline{\varepsilon}} = \left(\begin{array}{cc} \varepsilon_{xx} & \varepsilon_{xy} \\ \varepsilon_{xy} & \varepsilon_{yy} \end{array} \right). \tag{7.2}$$

Call λ_i the eigenvalues of $\underline{\underline{\varepsilon}}$. Then according to [6] the maximal distortional strain γ_{max} is defined as

$$\gamma_{max} := \frac{1}{2}|\lambda_1 - \lambda_2|. \tag{7.3}$$

The pore velocity (ν_{vel}) is related to the Darcy flux (q) and the porosity (n). The flux is divided by the porosity to account for the fact that only a fraction of the total formation volume is available for flow [13]. The fluid velocity is given by

$$\nu_{vel} = \frac{q}{n} = -\frac{\kappa}{n\zeta}\nabla p, \tag{7.4}$$

where κ is the permeability and ζ the viscosity. The shear strain and the fluid velocity will be calculated by equations for poro-elasticity.

7.1   Derivation of the poro-elastic equations

To derive the poro-elastic model, the following system of equations must be satisfied [14]:

$$\text{equilibrium equation}: \quad \text{div}\sigma - \nabla p = 0, \tag{7.5}$$

$$\text{constitutive equation}: \quad \sigma_{ij} = \lambda\delta_{ij}\varepsilon_{ll} + 2\mu\varepsilon_{ij}, \tag{7.6}$$

$$\text{compatibility condition}: \quad \varepsilon_{ij} = \frac{1}{2}(\partial_j u_i + \partial_i u_j), \tag{7.7}$$

$$\text{Darcy's law}: \quad \underline{q} = -\frac{\kappa}{\zeta}\nabla p, \tag{7.8}$$

$$\text{continuity equation}: \quad \nabla \cdot \underline{q} + \nabla \cdot \underline{\dot{u}} = f. \tag{7.9}$$

Here, λ and μ represent the Lamé constants.
Componentwisely, the equilibrium equation (7.5) is given by

$$\frac{\partial \sigma_{xx}}{\partial x} + \frac{\partial \sigma_{xy}}{\partial y} - \frac{\partial p}{\partial x} = 0, \tag{7.10}$$

$$\frac{\partial \sigma_{xy}}{\partial x} + \frac{\partial \sigma_{yy}}{\partial y} - \frac{\partial p}{\partial y} = 0. \tag{7.11}$$

The constitutive equations (7.6) imply that the above equations can be written as

$$\frac{\partial}{\partial x}\left((\lambda + 2\mu)\varepsilon_{xx} + \lambda\varepsilon_{yy}\right) + \frac{\partial}{\partial y}\left(2\mu\varepsilon_{xy}\right) - \frac{\partial p}{\partial x} = 0,$$

$$\frac{\partial}{\partial x}\left(2\mu\varepsilon_{xy}\right) + \frac{\partial}{\partial y}\left((\lambda + 2\mu)\varepsilon_{yy} + \lambda\varepsilon_{xx}\right) - \frac{\partial p}{\partial y} = 0.$$

By substituting the compatibility condition (7.7) the following is obtained

$$\frac{\partial}{\partial x}\left((\lambda + 2\mu)\frac{\partial u}{\partial x} + \lambda\frac{\partial v}{\partial y}\right) + \frac{\partial}{\partial y}\left(\mu\frac{\partial u}{\partial y} + \mu\frac{\partial v}{\partial x}\right) - \frac{\partial p}{\partial x} = 0,$$

$$\frac{\partial}{\partial x}\left(\mu\frac{\partial u}{\partial y} + \mu\frac{\partial v}{\partial x}\right) + \frac{\partial}{\partial y}\left((\lambda + 2\mu)\frac{\partial v}{\partial y} + \lambda\frac{\partial u}{\partial x}\right) - \frac{\partial p}{\partial y} = 0.$$

A further rearrangement of the above equations gives

$$(\lambda + \mu)\frac{\partial}{\partial x}\left(\frac{\partial u}{\partial x} + \frac{\partial v}{\partial y}\right) + \mu\Delta u - \frac{\partial p}{\partial x} = 0, \tag{7.12}$$

$$(\lambda + \mu)\frac{\partial}{\partial y}\left(\frac{\partial u}{\partial x} + \frac{\partial v}{\partial y}\right) + \mu\Delta v - \frac{\partial p}{\partial y} = 0, \tag{7.13}$$

or in vector notation

$$(\lambda + \mu)\nabla\left(\text{div}\underline{u}\right) + \mu\Delta\underline{u} - \nabla p = \underline{0}. \tag{7.14}$$

These are the first equations of the poro-elastic model.

From the mass-balance equation

$$\frac{\partial \rho^{\alpha}}{\partial t} + \nabla \cdot (\underline{\dot{u}}^{\alpha}\rho^{\alpha}) = Q^{\alpha},$$

it follows

$$\frac{\partial \rho^s}{\partial t} + \nabla \cdot (\underline{\dot{u}}^s \rho^s) = Q^s, \tag{7.15}$$

$$\frac{\partial \rho^f}{\partial t} + \nabla \cdot (\underline{\dot{u}}^f \rho^f) = Q^f. \tag{7.16}$$

Assuming no chemical interaction between the constituents implies $Q^\alpha = 0$. Furthermore, the density of a constituent α, ρ^α, is defined per unit volume V and actually represents an 'apparent' density. The true density ρ_*^α is defined per unit volume of the constituent V^α so

$$\rho^\alpha = n^\alpha \rho_*^\alpha, \qquad \text{with} \quad n^\alpha = \frac{V^\alpha}{V}.$$

It is assumed that the solid part is incompressible [6], $\dot{\rho}^s = 0$, and that the fluid part is slightly compressible according to

$$\dot{\rho}^f = \beta^f \rho^f \dot{p},$$

where β^f is the compressibility, which is equal to $1/K$, with K the bulk modulus. Then (7.15) and (7.16) become

$$\begin{aligned}
\nabla \cdot (\underline{\dot{u}}^s \rho^s) &= \nabla \cdot (\underline{\dot{u}}^s n^s \rho_*^s) \\
&= \nabla \cdot (\underline{\dot{u}}^s (1 - n^f) \rho_*^s) = 0,
\end{aligned}$$

$$\begin{aligned}
\frac{\partial \rho^f}{\partial t} + \nabla \cdot (\underline{\dot{u}}^f \rho^f) &= n^f \dot{\rho}_*^f + \nabla \cdot (\underline{\dot{u}}^f n^f \rho_*^f) \\
&= n^f \beta^f \rho_*^f \dot{p} + \nabla \cdot (\underline{\dot{u}}^f n^f \rho_*^f) \\
&= n^f \beta^f \dot{p} + \nabla \cdot (\underline{\dot{u}}^f n^f) \\
&= n^f \frac{\dot{\rho}_*^f}{\rho_*^f} + \nabla \cdot (\underline{\dot{u}}^f n^f) = 0.
\end{aligned}$$

Taking the sum leads to

$$n^f \beta^f \dot{p} + \nabla \cdot (\underline{\dot{u}}^f n^f) + \nabla \cdot (\underline{\dot{u}}^s (1 - n^f)) = 0,$$

so

$$n^f \beta^f \dot{p} + \nabla \cdot (\underline{\dot{u}}^f - \underline{\dot{u}}^s) n^f + \nabla \cdot (\underline{\dot{u}}^s) = 0.$$

Applying $n^f (\underline{\dot{u}}^f - \underline{\dot{u}}^s) = -\frac{\kappa}{\zeta}(\nabla p + \rho g)$, which follows from Darcy's law (7.8) and the continuity equation (7.9) gives

$$n^f \beta^f \dot{p} - \nabla \cdot (\frac{\kappa}{\zeta}(\nabla p + \rho g) + \nabla \cdot \underline{\dot{u}}^s) = 0.$$

Leaving out the gravity term

$$\frac{\partial}{\partial t}(n^f \beta^f p + \nabla \cdot \underline{u}^s) - \frac{\kappa}{\zeta}\Delta p = 0. \tag{7.17}$$

When assuming an incompressible fluid, the equation becomes

$$\frac{\partial}{\partial t}(\nabla \cdot \underline{u}^s) - \frac{\kappa}{\zeta}\Delta p = 0. \tag{7.18}$$

So the system follows from (7.14) and (7.17) for a slightly compressible fluid

$$-\mu\Delta\underline{u} - (\lambda + \mu)\nabla(\nabla \cdot \underline{u}) + \nabla p = \underline{0}, \tag{7.19}$$

$$n\beta\dot{p} + \nabla \cdot \underline{\dot{u}} - \frac{\kappa}{\zeta}\Delta p = 0, \tag{7.20}$$

and from (7.14) and (7.18) for an incompressible fluid

$$-\mu\Delta\underline{u} - (\lambda + \mu)\nabla(\nabla \cdot \underline{u}) + \nabla p = \underline{0}, \tag{7.21}$$

$$\nabla \cdot \underline{\dot{u}} - \frac{\kappa}{\zeta}\Delta p = 0. \tag{7.22}$$

7.2 Properties and conditions

The constants λ and μ are the Lamé constants, which are functions of the Young modulus E and the Poisson ratio ν

$$\lambda = \frac{E\nu}{(1 + \nu)(1 - 2\nu)}, \quad \mu = \frac{E}{2(1 + \nu)}. \tag{7.23}$$

The Young modulus of the prosthesis is different when bone has grown in, than when the prothesis only contains granulation tissue. The average elastic properties of the porous tantalum filled with fibrocartilage or fibrous tissue were taken as properties of the porous tantalum alone, because the latter is much stiffer than the filling soft tissues [6].

$$E_{porous\ tantalum+cart/fibr.tissue} = E_{porous\ tantalum}.$$

$$\nu_{porous\ tantalum+cart/fibr.tissue} = \nu_{porous\ tantalum}.$$

The elastic properties of the porous tantalum filled with bone were determined from the micro finite element voxel model, developed for this purpose [6]. The average *permeability* of porous tantalum, filled with bone, fibrous tissue and fibrocartilage is approximately determined based on the fact that permeability of porous tantalum alone is very high compared to the permeability of the filling tissues. So the average permeability of the whole material is mainly determined by the permeability of the filling tissue. Hence, the following assumption is used: The total permeability can be estimated as the permeability of the filling tissue multiplied by the its fraction in the porous tantalum, with the porosity of the porous tantalum being 0.82.

So with porosity of the porous tantalum layer being 0.82 and ζ being the viscosity

$$\left(\frac{\kappa}{\zeta}\right)_{bone+porous\ tantalum} = \left(\frac{\kappa}{\zeta}\right)_{bone} \cdot 0.82$$

$$= 3.7 \cdot 10^{-13}\frac{m^4}{Ns} \cdot 0.82 = 3.034 \cdot 10^{-13}\frac{m^4}{Ns}$$

$$\left(\frac{\kappa}{\zeta}\right)_{cart.+porous\ tantalum} = \left(\frac{\kappa}{\zeta}\right)_{cart.} \cdot 0.82$$

$$= 5.0 \cdot 10^{-15} \frac{m^4}{Ns} \cdot 0.82 = 4.1 \cdot 10^{-15} \frac{m^4}{Ns}$$

$$\left(\frac{\kappa}{\zeta}\right)_{fibr.+porous\ tantalum} = \left(\frac{\kappa}{\zeta}\right)_{fibr.} \cdot 0.82$$

$$= 1.0 \cdot 10^{-14} \frac{m^4}{Ns} \cdot 0.82 = 8.2 \cdot 10^{-15} \frac{m^4}{Ns}$$

Further for the porosity it is assumed

$$n_{porous\ tantalum+tissue} = n_{porous\ tantalum}$$

The values of the elastic properties in the porous tantalum will be computed according to the rule

$$E = E_{bone+poroustantalum}m_b + E_{cart.+poroustantalum}m_c + E_{fibr.+poroustantalum}m_f$$

$$\nu = \nu_{bone+poroustantalum}m_b + \nu_{cart.+poroustantalum}m_c + \nu_{fibr.+poroustantalum}m_f$$

$$\kappa = E_{bone+poroustantalum}m_b + \kappa_{cart.+poroustantalum}m_c + \kappa_{fibr.+poroustantalum}m_f$$

The mechanical properties are given by Table 7.1.

Material	E (MPa)	ν	$\frac{\kappa}{\zeta}(\frac{m^4}{Ns})$	n	K (MPa)
Por. Tant. with fibr. tissue	3300	0.31	$8.2 \cdot 10^{-15}$	0.82	2300
Por. Tant. with cartilage	3300	0.31	$4.1 \cdot 10^{-15}$	0.82	2300
Por. Tant. with bone	5000	0.35	$3.034 \cdot 10^{-13}$	0.82	2300

Table 7.1: Mechanical properties of porous tantalum filled with fibrous tissue, cartilage or bone.

For the grid, see Figure 7.1, the following conditions hold:
At Ω_1, the polyethylene part of the prosthesis, an elastic model holds. This means the pressure term is not present there. Ω_2 is represented by the poro-elastic equations.
For the boundaries the following conditions hold: On the implant interface Γ_3 a free fluid flow is assumed and the other boundaries of the porous tantalum layer are assumed to be impermeable. Further it is assumed a load of intensity is applied to the prosthesis by the humerus (at Γ_1). The load under an arm abduction of 30 degrees is applied to area d_2, the load under an arm abduction of 90 degrees is applied to area d_1.

$$\text{pressure} \quad : \quad \Gamma_{\bar{\Omega}_1 \cap \bar{\Omega}_2} : \quad \frac{\partial p}{\partial n} = 0, \tag{7.24}$$

$$\Gamma_2 : \quad \frac{\partial p}{\partial n} = 0, \tag{7.25}$$

$$\Gamma_3 : \quad p = 0. \tag{7.26}$$

$$\text{displacement} \quad : \quad \Gamma_1 : \quad \sigma = -\sigma_0, \tag{7.27}$$

$$\Gamma_2 : \quad \sigma = 0, \tag{7.28}$$

$$\Gamma_3 : \quad u = 0. \tag{7.29}$$

The loads applied to the prosthesis can be found in Table 7.2.
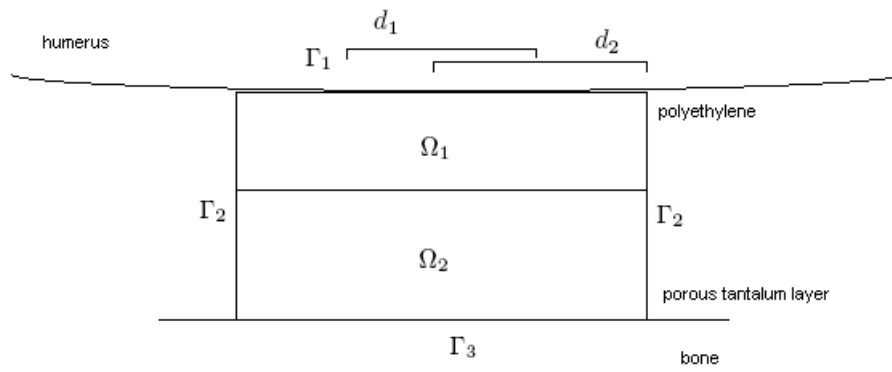
Figure 7.1: The geometry of the Bone-Implant interface.

force	arm abduction
165.84 N	30 degrees
325.85 N	60 degrees
392.85 N	90 degrees

Table 7.2: Applied forces

Chapter 8

Numerical methods

Now the FEM can be applied to the system of equations (7.14) and (7.17).

8.1 Weak formulation

First the weak formulation will be determined. For the first equation it follows

$$-\mu \text{div} \nabla u - (\lambda + \mu) \frac{\partial}{\partial x} \left(\frac{\partial u}{\partial x} + \frac{\partial v}{\partial y} \right) + \frac{\partial p}{\partial x} = 0,$$

or

$$-\mu \frac{\partial^2 u}{\partial x^2} - \mu \frac{\partial^2 u}{\partial y^2} - (\lambda + \mu) \frac{\partial^2 u}{\partial x^2} - (\lambda + \mu) \frac{\partial^2 v}{\partial x \partial y} + \frac{\partial p}{\partial x} = 0,$$

and rearranging terms gives

$$-\frac{\partial}{\partial x} \left((\lambda + 2\mu) \frac{\partial u}{\partial x} + \lambda \frac{\partial v}{\partial y} \right) - \frac{\partial}{\partial y} \left(\mu \frac{\partial u}{\partial y} + \mu \frac{\partial v}{\partial x} \right) + \frac{\partial p}{\partial x} = 0.$$

The weak formulation is given by

$$\int_\Omega \eta \left[-\frac{\partial}{\partial x} \left((\lambda + 2\mu) \frac{\partial u}{\partial x} + \lambda \frac{\partial v}{\partial y} \right) - \frac{\partial}{\partial y} \left(\mu \frac{\partial u}{\partial y} + \mu \frac{\partial v}{\partial x} \right) + \frac{\partial p}{\partial x} \right] d\Omega = 0,$$

and apply the Gauss-Green theorem [15]

$$-\int_\Gamma \eta \left[\left((\lambda + 2\mu) \frac{\partial u}{\partial x} + \lambda \frac{\partial v}{\partial y} \right) n_x + \left(\mu \frac{\partial u}{\partial y} + \mu \frac{\partial v}{\partial x} \right) n_y \right] d\Gamma \qquad (8.1)$$

$$+ \int_\Omega \frac{\partial \eta}{\partial x} \left((\lambda + 2\mu) \frac{\partial u}{\partial x} + \lambda \frac{\partial v}{\partial y} \right) + \frac{\partial \eta}{\partial y} \left(\mu \frac{\partial u}{\partial y} + \mu \frac{\partial v}{\partial x} \right) d\Omega + \int_\Omega \eta \frac{\partial p}{\partial x} d\Omega = 0.$$

At Γ_3 a Dirichlet boundary is prescribed, so η is zero there. At the other boundaries forces are applied. On the surface the following equations hold for the

applied forces [15]

$$
\begin{aligned}
q_x &= \sigma_{xx}n_x + \sigma_{xy}n_y \\
&= \left((\lambda+2\mu)\frac{\partial u}{\partial x} + \lambda\frac{\partial v}{\partial y}\right)n_x + \left(\mu\frac{\partial u}{\partial y} + \mu\frac{\partial v}{\partial x}\right)n_y, \\
q_y &= \sigma_{xy}n_x + \sigma_{yy}n_y \\
&= \left(\mu\frac{\partial v}{\partial x} + \mu\frac{\partial u}{\partial y}\right)n_x + \left((\lambda+2\mu)\frac{\partial v}{\partial y} + \lambda\frac{\partial u}{\partial x}\right)n_y.
\end{aligned}
$$

Apply this to (8.1) and it follows

$$
-\int_{\Gamma_1+\Gamma_2}\eta q_x d\Gamma + \int_\Omega \frac{\partial\eta}{\partial x}\left((\lambda+2\mu)\frac{\partial u}{\partial x}+\lambda\frac{\partial v}{\partial y}\right)
$$
$$
+\frac{\partial\eta}{\partial y}\left(\mu\frac{\partial u}{\partial y}+\mu\frac{\partial v}{\partial x}\right)d\Omega + \int_\Omega \eta\frac{\partial p}{\partial x}d\Omega = 0. \tag{8.2}
$$

Following the same procedure for the second equation leads to

$$
-\int_{\Gamma_1+\Gamma_2}\eta q_y d\Gamma + \int_\Omega \frac{\partial\eta}{\partial x}\left(\mu\frac{\partial u}{\partial y}+\mu\frac{\partial v}{\partial x}\right)
$$
$$
+\frac{\partial\eta}{\partial y}\left(\lambda\frac{\partial u}{\partial x}+(\lambda+2\mu)\frac{\partial v}{\partial y}\right)d\Omega + \int_\Omega \eta\frac{\partial p}{\partial x}d\Omega = 0. \tag{8.3}
$$

For the third equation the weak formulation is derived as follows:

$$
\frac{d}{dt}\int_\Omega \eta n\beta p\, d\Omega + \frac{d}{dt}\int_\Omega\left(\frac{\partial u}{\partial x}+\frac{\partial v}{\partial y}\right)\eta\, d\Omega - \int_\Omega \eta\frac{\kappa}{\zeta}\Delta p\, d\Omega
$$
$$
= \int_\Omega \eta f(\underline{x},t)d\Omega.
$$

Substituting Robin boundary conditions $\frac{\kappa}{\zeta}\frac{\partial p}{\partial n} = k_B(p-p_B)$ leads to

$$
\frac{d}{dt}\int_\Omega \eta n\beta p\, d\Omega + \frac{d}{dt}\int_\Omega\left(\frac{\partial u}{\partial x}+\frac{\partial v}{\partial y}\right)\eta\, d\Omega + \int_\Omega \nabla\eta\frac{\kappa}{\zeta}\nabla p\, d\Omega - \int_\Gamma \eta k_B(p-p_B)d\Gamma
$$
$$
= \int_\Omega \eta f(\underline{x},t)d\Omega. \tag{8.4}
$$

8.2 Stabilization

If the FEM is used, choosing the same approximation space for the displacements and the pressure, can lead to strong oscillations in the approximation for the pressure [14]. Consider the weak formulations for an incompressible fluid

$$
-\int_{\Gamma_1+\Gamma_2}\eta q_x d\Gamma + \int_\Omega \frac{\partial\eta}{\partial x}\left((\lambda+2\mu)\frac{\partial u}{\partial x}+\lambda\frac{\partial v}{\partial y}\right)
$$
$$
+\frac{\partial\eta}{\partial y}\left(\mu\frac{\partial u}{\partial y}+\mu\frac{\partial v}{\partial x}\right)d\Omega + \int_\Omega \eta\frac{\partial p}{\partial x}d\Omega = 0
$$

$$-\int_{\Gamma_1+\Gamma_2} \eta q_y d\Gamma + \int_\Omega \frac{\partial \eta}{\partial x}\left(\mu\frac{\partial u}{\partial y} + \mu\frac{\partial v}{\partial x}\right)d\Omega + \frac{\partial \eta}{\partial y}\left(\lambda\frac{\partial u}{\partial x} + (\lambda + 2\mu)\frac{\partial v}{\partial y}\right)d\Omega$$
$$+ \int_\Omega \eta\frac{\partial p}{\partial x}d\Omega = 0.$$

$$\frac{d}{dt}\int_\Omega \left(\frac{\partial u}{\partial x} + \frac{\partial v}{\partial y}\right)\eta d\Omega + \int_\Omega \nabla\eta\frac{\kappa}{\zeta}\nabla p d\Omega - \int_\Gamma \eta k_B(p - p_B)d\Gamma$$
$$= \int_\Omega \eta f(\underline{x},t)d\Omega. \quad (8.5)$$

When $\dfrac{\kappa}{\zeta} \to 0$ the solution of this problem tends to the solution of

$$-\int_{\Gamma_1+\Gamma_2} \eta q_x d\Gamma + \int_\Omega \frac{\partial \eta}{\partial x}\left((\lambda + 2\mu)\frac{\partial u}{\partial x} + \lambda\frac{\partial v}{\partial y}\right)$$
$$+ \frac{\partial \eta}{\partial y}\left(\mu\frac{\partial u}{\partial y} + \mu\frac{\partial v}{\partial x}\right)d\Omega + \int_\Omega \eta\frac{\partial p}{\partial x}d\Omega = 0, \quad (8.6)$$

$$-\int_{\Gamma_1+\Gamma_2} \eta q_y d\Gamma + \int_\Omega \frac{\partial \eta}{\partial x}\left(\mu\frac{\partial u}{\partial y} + \mu\frac{\partial v}{\partial x}\right)d\Omega + \frac{\partial \eta}{\partial y}\left(\lambda\frac{\partial u}{\partial x} + (\lambda + 2\mu)\frac{\partial v}{\partial y}\right)d\Omega$$
$$+ \int_\Omega \eta\frac{\partial p}{\partial x}d\Omega = 0. \quad (8.7)$$

$$\frac{d}{dt}\int_\Omega \left(\frac{\partial u}{\partial x} + \frac{\partial v}{\partial y}\right)\eta d\Omega = \int_\Omega \eta f(\underline{x},t)d\Omega. \quad (8.8)$$

To derive the Galerkin equations, two types of basis functions are defined: one for the pressure $\psi_i(\underline{x})$ and one for the velocity components $\phi_i(\underline{x})$. Further holds $u^n = \sum_{j=1}^n u_j(t)\phi_j(\underline{x})$, $v^n = \sum_{j=1}^n v_j(t)\phi_j(\underline{x})$ and $p^n = \sum_{j=1}^n p_j(t)\psi_j(\underline{x})$.

Substitution in 8.6)-(8.8) leads to

$$-\int_{\Gamma_1+\Gamma_2} \phi_i q_x d\Gamma + \int_\Omega \frac{\partial \phi_i}{\partial x}\left((\lambda + 2\mu)\frac{\partial u_j\phi_j}{\partial x} + \lambda\frac{\partial v_j\phi_j}{\partial y}\right)$$
$$+ \frac{\partial \phi_i}{\partial y}\left(\mu\frac{\partial u_j\phi_j}{\partial y} + \mu\frac{\partial v_j\phi_j}{\partial x}\right)d\Omega + \int_\Omega \phi_i\frac{\partial p_j\psi_j}{\partial x}d\Omega = 0, \quad (8.9)$$

$$-\int_{\Gamma_1+\Gamma_2} \eta q_y d\Gamma + \int_\Omega \frac{\partial \phi_i}{\partial x}\left(\mu\frac{\partial u_j\phi_j}{\partial y} + \mu\frac{\partial v_j\phi_j}{\partial x}\right)d\Omega +$$
$$\frac{\partial \phi_i}{\partial y}\left(\lambda\frac{\partial u_j\phi_j}{\partial x} + (\lambda + 2\mu)\frac{\partial v_j\phi_j}{\partial y}\right)d\Omega + \int_\Omega \phi_i\frac{\partial p_j\psi_i}{\partial x}d\Omega = 0. \quad (8.10)$$

$$\frac{d}{dt}\int_\Omega \left(\frac{\partial u_j \phi_j}{\partial x} + \frac{\partial v_j \phi_j}{\partial y}\right)\psi_i d\Omega = \int_\Omega \eta f(\underline{x},t)d\Omega. \qquad (8.11)$$

Equation (8.11) does not contain a pressure term, so a problem arises.

The number of rows is completely determined by the number of pressure unknowns [16]. So if the number of pressure unknowns exceeds the number of velocity unknowns, the matrix of the system to be solved contains more rows than unknowns so the system is either dependent or inconsistent and the matrix is singular. So the number of pressure unknowns may never exceed the number of velocity unknowns.

This should hold on various grid sizes so this should hold independently of the number of elements. For that reason the number of applicable elements is reduced. There is an exact admissibility condition, the so called Ladyzenskaya-Brezzi-Babuska condition. This condition is fulfilled if the following holds [16]:

Given a continuous differentiable vector field $\underline{u}$ and basis function ψ_i. If one can explicitly build a discrete vector field $\underline{\tilde{u}}$ such that

$$\int_\Omega \psi_i \mathrm{div}\underline{\tilde{u}}d\Omega = \int_\Omega \psi_i \mathrm{div}\underline{u}d\Omega, \quad \forall \quad \psi_i, \qquad (8.12)$$

then the LBB-condition is satisfied.

Frequently elements are used that do not satisfy this condition, because it is very difficult to verify if this constraint is satisfied.

An example of admissible elements are the Taylor-Hood elements: when the velocity is approximated by a polynomial of degree k, then the pressure will be approximated by a polynomial of degree $k-1$. It is proved this element is admissible if at least three elements are used [16]. However, there are strong constraints for the discretisation parameters to fulfill [14], otherwise there can still occur oscillatory behaviour.

Another way to suppress the wiggles is presented by Aguilar et al [14]. The idea is to reformulate the poro elastic problem in such a way that the transformed problem only involves Laplace operators. Then finally from discretising this transformed problem on a collocated grid, a perturbed discrete variant of the original problem can be derived, leading to

$$-\mu\Delta\underline{u} - (\lambda+\mu)\nabla(\nabla\cdot\underline{u}) + \nabla p = \underline{0} \qquad (8.13)$$

$$\nabla\cdot\underline{\dot{u}} - \frac{\kappa}{\zeta}\Delta p - \beta_s\Delta\dot{p} = 0, \qquad (8.14)$$

where $\beta_s\Delta\dot{p}$ is the stabilization term. Small perturbations of this stabilization parameter β_s results in excess of the numerical diffusion [14].

In this case a big limitation appears because the strategy requires a good choice of the stabilization parameter. If the value is too large the problem will be over-stabilized. The best value for the parameter β_s in the one-dimensional case is $\beta_s = \frac{h^2}{4(\lambda + 2\mu)}$.

8.3   Galerkin equations

Now the Galerkin equations can be derived. For both the pressure term as for
the displacement terms a linear basis function will be used.

First equation

$$-\int_{\Gamma_1+\Gamma_2} \phi_i q_x d\Gamma + \sum_{j=1}^{n} \int_{\Omega} \frac{\partial \phi_i}{\partial x}\left((\lambda+2\mu)\frac{\partial \phi_j}{\partial x}u_j + \lambda\frac{\partial \phi_j}{\partial y}v_j\right) \qquad (8.15)$$

$$+\frac{\partial \phi_i}{\partial y}\left(\mu\frac{\partial \phi_j}{\partial y}u_j + \mu\frac{\partial \phi_j}{\partial x}v_j\right) d\Omega + \sum_{j=1}^{n} \int_{\Omega} \phi_i \frac{\partial \phi_j}{\partial x}p_j d\Omega \quad = \quad 0.$$

Next the integrals will be computed elementwisely, following the same proce-
dure as in Section 3.1. An assembly procedure is applied to generate the global
matrices that are involved in the Finite Element discretisation.
Then for the first integral of (8.15), the 2×1 boundary element vector is given
by

$$Bf_u^{el} = -\frac{|\triangle|}{2}q_x$$

For the second integral of (8.15) the 3×3 element matrix follows

$$Z_{uu}^{el} = \frac{|\triangle|}{2}((\lambda+2\mu)a_1^i a_1^j + \mu a_2^i a_2^j),$$

$$Z_{uv}^{el} = \frac{|\triangle|}{2}(\lambda a_1^i a_2^j + \mu a_1^j a_2^i),$$

and the last integral leads to the 3×3 element matrix

$$Z_{up}^{el} = \frac{|\triangle|}{6}a_1^j.$$

Second equation   Following the same procedure, the 3×3 element matrices,
for the second equation are given by

$$Z_{vv}^{el} = \frac{|\triangle|}{2}(\mu a_1^i a_1^j + (\lambda+2\mu)a_2^i a_2^j),$$

$$Z_{vu}^{el} = \frac{|\triangle|}{2}(\lambda a_2^i a_1^j + \mu a_1^i a_2^j),$$

$$Z_{vp}^{el} = \frac{|\triangle|}{6}a_2^j,$$

to be used in the assembly procedure for the stiffnessmatrix Z.
And the 2×1 boundary element vector

$$Bf_v^{el} = -\frac{|\triangle|}{2}q_y,$$

to be used in the assembly procedure for the vector f.

Third equation For now, the slightly compressible term and the stability term are both present, just to show the discretisation of both. Of course, for an incompressible fluid $\beta_s = 0$ holds, and for an incompressible fluid with stabilization term $\beta = 0$ holds.
The equation reads

$$n\beta\dot{p} + \nabla \cdot \underline{\dot{u}} - \frac{\kappa}{\zeta}\Delta p - \beta_s\Delta\dot{p} = f(\underline{x}, t).$$

The weak formulation is given by

$$\frac{d}{dt}\int_\Omega \eta n\beta p d\Omega + \frac{d}{dt}\int_\Omega \left(\frac{\partial u}{\partial x} + \frac{\partial v}{\partial y}\right)\eta d\Omega + \int_\Omega \nabla\eta\frac{\kappa}{\zeta}\nabla p d\Omega - \int_\Gamma \eta k_B(p - p_B)d\Gamma$$

$$- \int_\Omega \eta\beta_s\Delta\dot{p}d\Omega = \int_\Omega \eta f(\underline{x}, t)d\Omega.$$

Setting $u(x, y, t) = \sum_{j=1}^{n} u_j(t)\phi_j(x, y)$ and $v(x, y, t) = \sum_{j=1}^{n} v_j(t)\phi_j(x, y)$ gives

$$\sum_{j=1}^{n} p_j'(t)\int_\Omega n\beta\phi_i\phi_j d\Omega + \sum_{j=1}^{n} u_j'(t)\int_\Omega \phi_i\frac{\partial\phi_j}{\partial x}d\Omega + \sum_{j=1}^{n} v_j'(t)\int_\Omega \phi_i\frac{\partial\phi_j}{\partial y}d\Omega$$

$$+ \sum_{j=1}^{n} p_j(t)\int_\Omega \frac{\kappa}{\zeta}\nabla\phi_i \cdot \nabla\phi_j d\Omega - \sum_{j=1}^{n} p_j(t)\int_\Gamma \phi_i k_B\phi_j d\Gamma + \int_\Gamma \phi_i k_B p_B d\Gamma$$

$$+ \sum_{j=1}^{n} p_j'(t)\int_\Omega \beta_s\nabla\phi_i \cdot \nabla\phi_j d\Omega - \sum_{j=1}^{n} p_j'(t)\int_\Gamma \beta_s\frac{\zeta}{\kappa}\phi_i k_B\phi_j + \int_\Gamma \beta_s\frac{\zeta}{\kappa}\phi_i k_B p_B$$

$$= \int_\Omega f\phi_i d\Omega$$

Applying Euler Backward time-discretisation yields

$$
\sum_{j=1}^{n} p_j^{k+1} \int_{\Omega} n\beta\phi_i\phi_j d\Omega + \sum_{j=1}^{n} u_j^{k+1} \int_{\Omega} \phi_i \frac{\partial\phi_j}{\partial x} d\Omega + \sum_{j=1}^{n} v_j^{k+1} \int_{\Omega} \phi_i \frac{\partial\phi_j}{\partial y} d\Omega
$$

$$
+ \sum_{j=1}^{n} \Delta t p_j^{k+1} \int_{\Omega} \frac{\kappa}{\eta} \nabla\phi_i \nabla\phi_j d\Omega - \sum_{j=1}^{n} \Delta t p_j^{k+1} \int_{\Gamma} \phi_i k_B \phi_j d\Gamma
$$

$$
+ \sum_{j=1}^{n} p_j^{k+1} \int_{\Omega} \beta_s \nabla\phi_i \cdot \nabla\phi_j d\Omega - \sum_{j=1}^{n} p_j^{k+1} \int_{\Gamma} \beta_s \frac{\zeta}{\kappa} \phi_i k_B \phi_j d\Gamma
$$

$$
= \sum_{j=1}^{n} p_j^{k} \int_{\Omega} n\beta\phi_i\phi_j d\Omega + \sum_{j=1}^{n} u_j^{k} \int_{\Omega} \phi_i \frac{\partial\phi_j}{\partial x} d\Omega + \sum_{j=1}^{n} v_j^{k} \int_{\Omega} \phi_i \frac{\partial\phi_j}{\partial y} d\Omega
$$

$$
+ \sum_{j=1}^{n} p_j^{k} \int_{\Omega} \beta_s \nabla\phi_i \cdot \nabla\phi_j d\Omega - \sum_{j=1}^{n} p_j^{k} \int_{\Gamma} \beta_s \frac{\zeta}{\kappa} \phi_i k_B \phi_j d\Gamma + \Delta t \int_{\Omega} f\phi_i d\Omega
$$

$$
- \int_{\Gamma} \phi_i k_B p_B d\Gamma. \tag{8.16}
$$

So in vector notation the final system for (8.2), (8.3), (8.4) looks like

$$
\begin{bmatrix} Z_{uu} & Z_{uv} & Z_{up} \\ Z_{vu} & Z_{vv} & Z_{vp} \\ Z_{pu} & Z_{pv} & Z_{pp} \end{bmatrix} \begin{bmatrix} \underline{u}^{k+1} \\ \underline{v}^{k+1} \\ \underline{p}^{k+1} \end{bmatrix} = \begin{bmatrix} 0 \\ 0 \\ Z_{pu}\underline{u}^k + Z_{pv}\underline{v}^k + Z_{pp}\underline{p}^k + \Delta t\underline{f}^k \end{bmatrix}
$$

$$
= \begin{bmatrix} 0 & 0 & 0 \\ 0 & 0 & 0 \\ Z_{pu} & Z_{pv} & Z_{pp} \end{bmatrix} \begin{bmatrix} \underline{u}^k \\ \underline{v}^k \\ \underline{p}^k \end{bmatrix} + \begin{bmatrix} \underline{0} \\ \underline{0} \\ \underline{f}^k \Delta t \end{bmatrix}.
$$

Next, the above integrals still have to be computed. This will be done following the same procedure as in Section 7.1. So applying Newton-Cotes to the integrals on the left-hand-side of (8.16), the 3×3 element matrix for the second integral, which contributes to Z_{pu}, looks like

$$
Z_{pu(ij)}^{el} = \int_{\Omega} \phi_i \frac{\partial\phi_j}{\partial x} d\Omega = \frac{|\triangle|}{6} a_1^j.
$$

For the third integral, contributing to Z_{pv}, the 3×3 element matrix is

$$
Z_{pv(ij)}^{el} = \frac{|\triangle|}{6} a_2^j,
$$

The first, fourth and fifth integral, which contribute to Z_{pp}, lead to the 3×3 element matrix

$$
Z_{pp(ij)}^{el} = \frac{|\triangle|}{2}(a_1^i a_1^j + a_2^i a_2^j)(\Delta t \frac{\kappa}{\zeta} + \beta_s) + \frac{|\triangle|}{6} n\beta\delta_{ij},
$$

The boundary integrals, which also contribute to Z_{pp}, lead to the 2×2 element matrix

$$
BM_{ij}^{el} - \frac{|\triangle|}{2} k_B(\Delta t + \beta_s \frac{\zeta}{\kappa})\delta_{ij}. \tag{8.17}
$$

The integrals on the right hand side can be computed following the same procedure. For the second and third integral this leads again to the 3×3 element matrices

$$Z_{pu(ij)}^{el} = \frac{|\triangle|}{6} a_1^j,$$

and

$$Z_{pv(ij)}^{el} = \frac{|\triangle|}{6} a_2^j,$$

The first and fourth integral lead to 3×3 element matrix

$$Z_{pp(ij)}^{el} = \frac{|\triangle|}{2} (a_1^i a_1^j + a_2^i a_2^j)\beta_s + \frac{|\triangle|}{6} n\beta\delta_{ij},$$

The fifth integral is a boundary integral, contributing to Z_{pp}, leading to the 2×2 element matrix

$$BM_{ij}^{el} = -\frac{|\triangle|}{2} \beta_s \frac{\zeta}{\kappa} k_B \delta_{ij}. \tag{8.18}$$

The other integrals contribute to the element vector and give the 3×1 vector

$$f_{ij}^{el} = \frac{|\triangle|}{2} f_i \Delta t,$$

and the 2×1 boundary element vector

$$Bf_{ij}^{el} = -\frac{|\triangle|}{2} k_B p_B \Delta t.$$

Chapter 9

Results

Now the whole model due to Prendergast can be simulated. The parameters used in the mechanical part of the model are stated in Section 7.2. Further holds $S_{min} = 1$ and $S_{max} = 3$. For the biological part the parameter values are:

$P_{mmin} = 0.5$, $P_{mmax} = 1.2$, $P_{fmin} = 0.1$, $P_{fmax} = 0.6$, $P_{cmin} = 0.75$, $P_{cmax} = 0.925$, $P_{bmin} = 0.5$, $P_{bmax} = 1.5 * P_{bmin}$, $F_{fmin} = 0$, $F_{fmax} = 0.01$, $F_{cmin} = 0$;, $F_{cmax} = 0.3$, $F_{bmin} = 0.005$, $F_{bmax} = 0.15$, $Q)fmin = 0$, $Q_{fmax} = 0.06$, $Q_{cmin} = 0$, $Q_{cmax} = 0.2$, $Q_{bmin} = 0.001$, $Q_{bmax} = 0.1$.

First some figures will be shown for the mechanical part.
Every iteration contains one update for the biological properties and one update for the mechanical properties. The process of cell-differentiation is a lot slower then the process of an arm abduction, which only lasts two seconds.
In Figure 9.1 the shear strain, fluid velocity and stimulus are shown under an arm abduction of 30 degrees after 1 iteration. The value of the fluid velocity will tends to zero if the applied load works at the same area with the same force. In that case the stimulus will be determined only by the shear strain and, as shown in Figure 9.1, will not be higher than 0.25. So, keeping the arm abduction the same under an angle of 30 degrees, during the whole simulation of 200 days, no cartilage or fibrous tissue will appear. Bone grows very slowly and only in the lower left corner, where the stimulus is highest, see Figure 9.2.

Under an arm abduction of 90 degrees, where the applied force is 392.95 N, the shearstrain, fluid velocity and stimulus after 1 iteration are shown in Figure 9.3. For the next simulation the following is assumptions are made: Every 3 days an arm abduction of 90 degrees is made, during the first 100 days. The stimulus that follows from this, is assumed to hold throughout the whole day. The rest of the time the arm abduction is kept at 30 degrees.
So, with $dt = 1\ day$ every third iteration the applied force is 392.95 N under an angle of 90 degrees, and for the other iterations the applied force is 165.84 N, under an angle of 30 degrees.
This way the fluid velocity will not drop to zero during the first 100 days and this gives an idea how the model works.
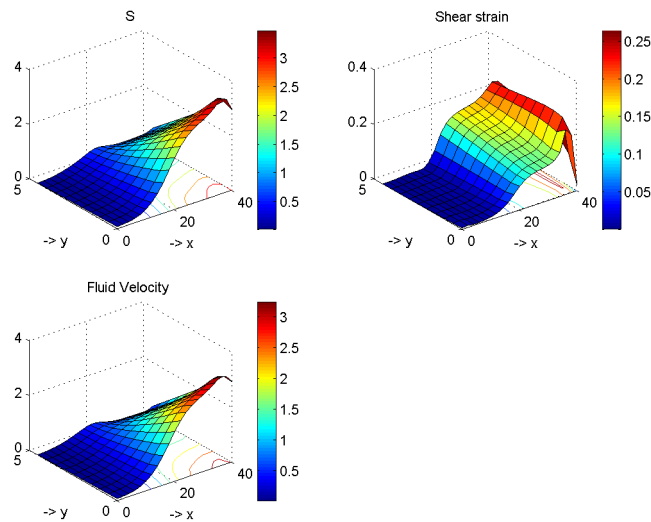
Figure 9.1: The maximal distortional strain (upper right picture), the fluid velocity (lower left picture) and the resulting stimulus (upper left picture), under an arm abduction of 30 degrees.

In Figure 9.4 bone appears only at the right and cartilage is formed in the middle. Fibrous tissue only appears at the right side of the implant interface. After 200 days the pattern looks pretty much the same. Only at the lower right corner the cartilage density decreased and a small concentration of bone has appeared. This is not very strange, since the arm abduction was kept at 30 degrees from day 100. It is known from Figures 9.1 and 9.2, that the stimulus is very low in that case and has the biggest contribution at the lower right corner of the grid.

The results seem to be determined mainly by the mechanical stimulus and the influence of the cell differentiation process seems almost neglectable. This is the case, because the cell differentiation becomes most important when the value for the stimulus is in the neighbourhood of $S = 1$ or $S = 3$, see Appendix A. Here however, the value of the stimulus at most areas is not close enough to $S = 1$ or $S = 3$ to let the differentiation process become important.
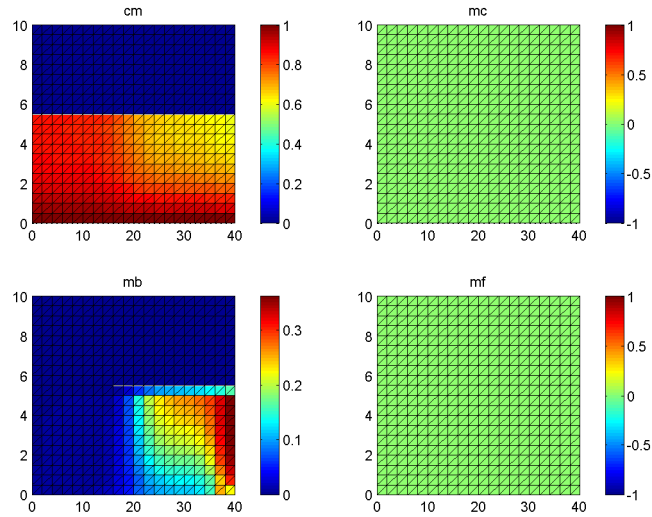
Figure 9.2: Mesenchymal cellular density (upper left picture) and matrix densities of cartilage (upper right picture), bone(lower left picture) and fibrous tissue (lower right picture).
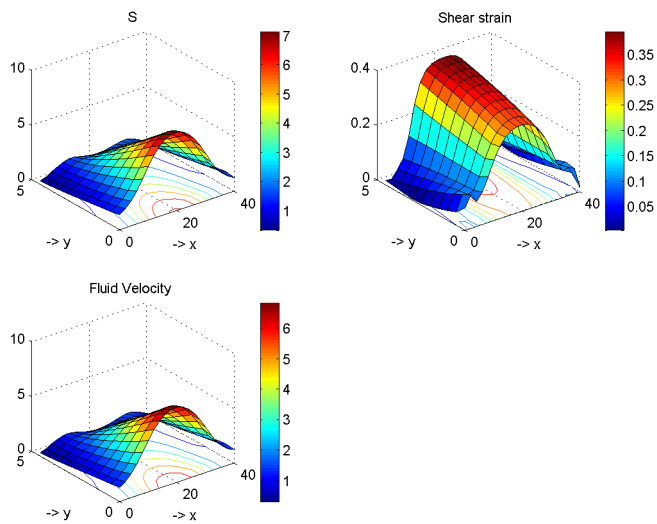
Figure 9.3: The maximal distortional strain (upper right picture), the fluid velocity (lower left picture) and the resulting stimulus (upper left picture), under an arm abduction of 90 degrees.
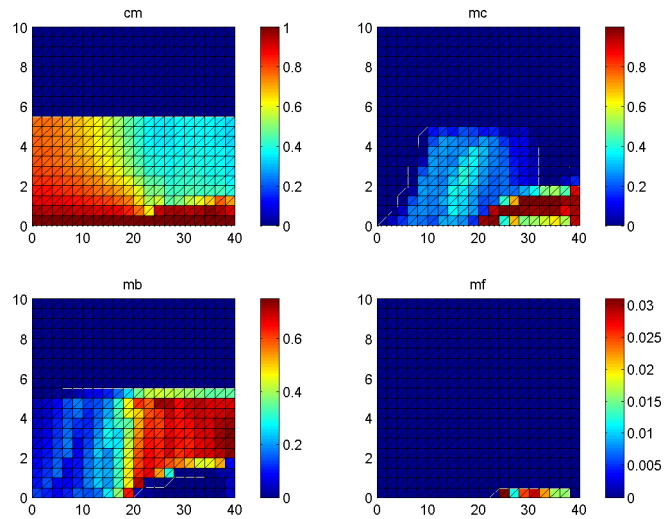
Figure 9.4: The mesenchymal cellular density (upper left picture) and the matrix densities after 100 days. In the upper right picture the cartilage density is shown, the lower left picture shows bone and the lower right picture represents fibrous tissue.
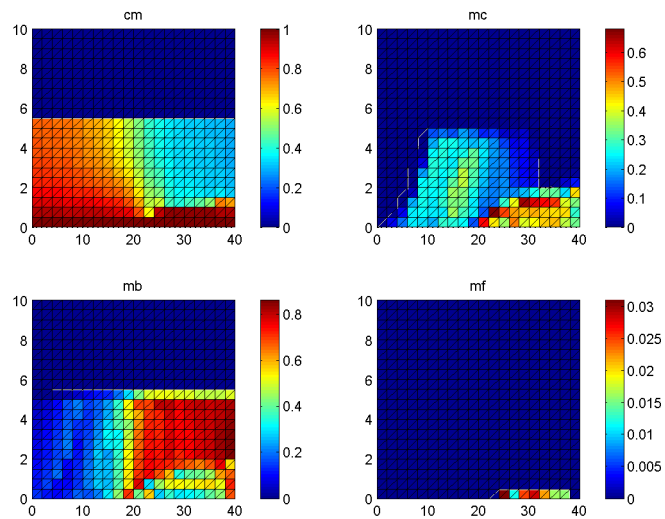
Figure 9.5: The mesenchymal cellular density (upper left) and the matrix densities after 200 days. In the upper right picture is the cartilage density shown, the lower left picture shows bone and lower right represents fibrous tissue.

Chapter 10

Conclusion

In this report the process of tissue differentiation during bone ingrowth into an shoulder prosthesis has been described. A comparison to the process of fracture healing has been made and two models to describe this process have been explained: the model due to Prendergast and the model due to Bailon-Plaza. A third model is briefly mentioned.

The model of Prendergast also contains of a mechanical part. The derivation of this part is shown. The mechanical part calculates the stimulus S, which influences the process of tissue differentiation. For $S < 1$ bone will appear, for $1 < S < 3$ cartilage and for $S > 3$ fibrous tissue will appear.

The biological part of the model due to Prendergast in 2-D has been implemented in MATLAB using the Finite Element Method and the (semi-implicit) Euler backward scheme. The result show how the tissue differentiation works when the stimulus, which comes from the mechanical part of the model, is constantly kept at 1. No fibrous tissue is made during the whole process. Cartilage appears first and after 30 days is decays and bone will grow into the prosthesis.

After that the fracture healing model of Bailon-Plaza has been implemented. In this model also growth factors have been taken into account. The parameters that seem to be of most influence on the bone growth process, are the decay factor of the bone growth factor and the production rate of bone matrix.

Then the mechanical part of the model of Prendergast was implemented. This showed that under an arm abduction of 30 degrees bone grows in is really slowly and no cartilage or fibrous tissue will be made. This is the case because the stimulus is very low. If cycles of arm abductions of both 30 degrees and 90 degrees are simulated, also cartilage and fibrous tissue will appear. The results seem to be determined mainly by the mechanical stimulus and less by the cell differentiation process. This can be explained by the fact that the tissue differentiation process only has a real influence when the value of the stimulus is close to either 1 or 3.

It would be nice to add equations for the growth factors, like seen in the model due to Bailon-Plaza, to the model due to Prendergast, since an abnormal distribution of growth factors might give other results of the bone growth into the prosthesis.

Also, since the process of tissue differentiation is a lot slower than the arm abduction from the mechanical part, which only lasts two seconds, smaller time steps could be chosen for improvement of the results.

Further in this report it is assumed that mesenchymal cells originate from the bone-implant interface, and this is kept at a maximal value c_{max}. However, if the interface micromotions [6] do not exceed a certain threshold, there will be no interface bonding and no mesenchymal cells will 'jump' into the prosthesis.

Appendix A

The proliferation rates P_{m0}, P_{f0}, P_{c0}, P_{b0}, differentiation rates F_f, F_c, F_b and production rates Q_f, Q_c, Q_b depend on the stimulus S in the following way, with $S_{min} = 1$ and $S_{max} = 3$:
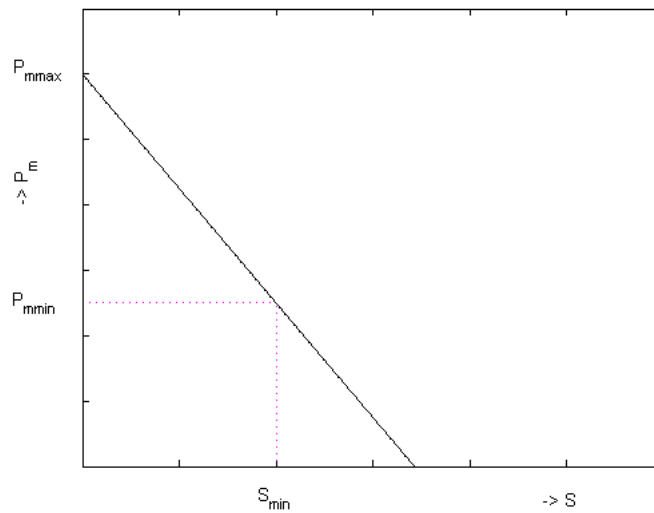
Figure A.1: The mesenchymal cell proliferation rate as a function of the stimulus S. The higher the stimulus, the lower the proliferation rate.

The production rates Q_f, Q_c, Q_b depend on the stimulus S in the same way that the differentiation rates F_f, F_c and F_b do.
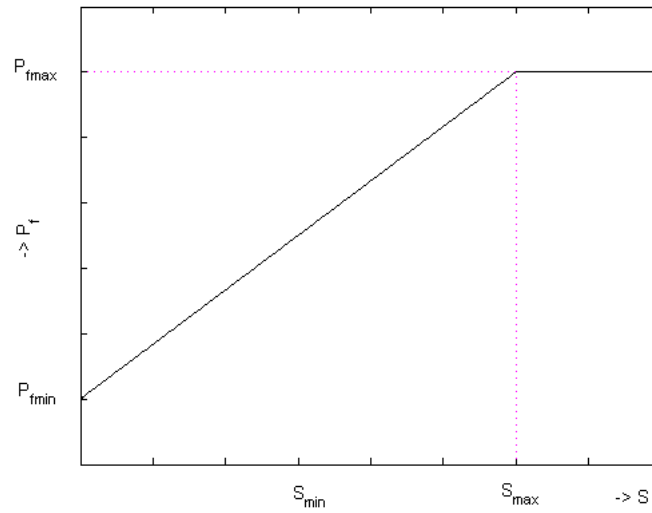
Figure A.2: The proliferation rate of fibroblasts as a function of the stimulus S. If S increases, then also P_{f0} increases.
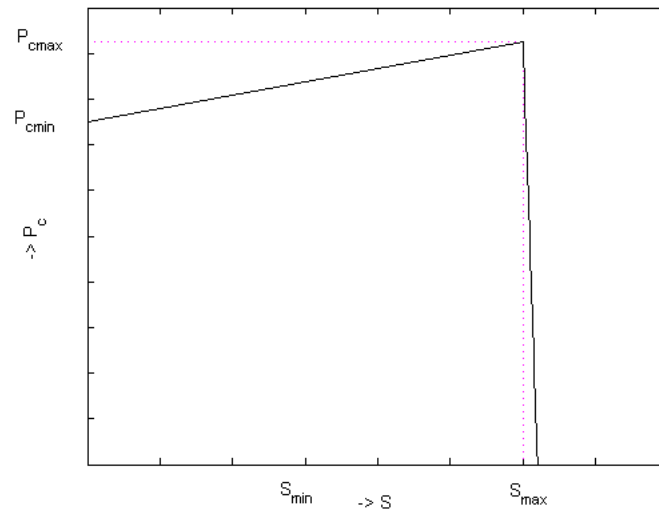
Figure A.3: The proliferation rate of chondrocytes as a function of the stimulus S. If S exceeds S_{max}, then P_{c0} becomes zero.
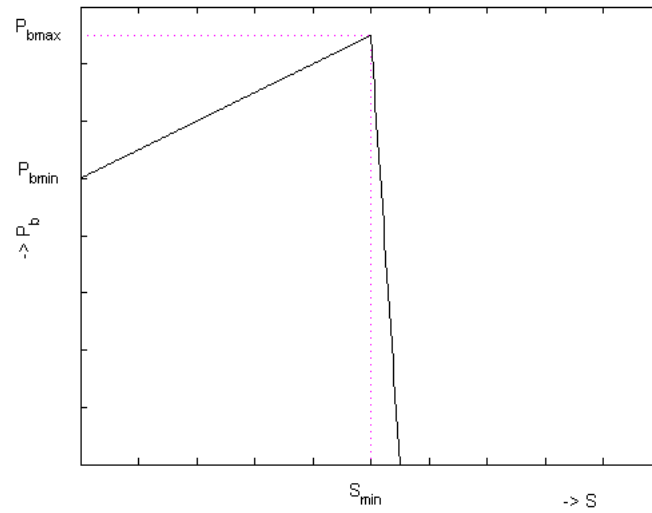
Figure A.4: The proliferation rate of osteoblasts as a function of the stimulus S. When S exceeds S_{min}, P_{b0} tends to zero.
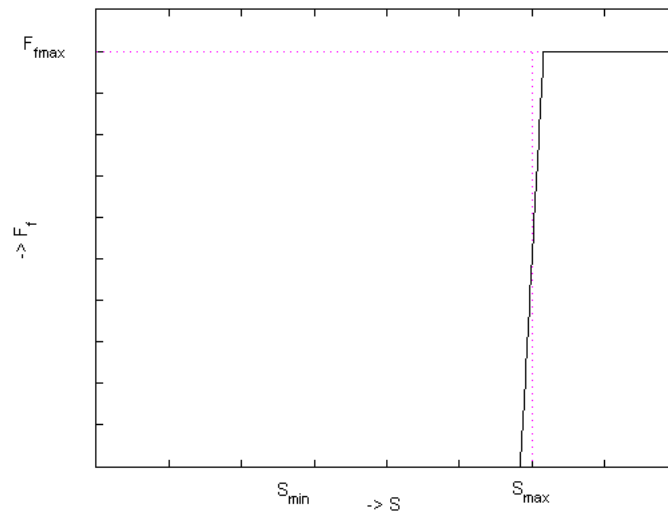
Figure A.5: The differentiation rate of fibroblasts as function of the stimulus S. If the stimulus does not exceed a threshold, F_f stays zero.
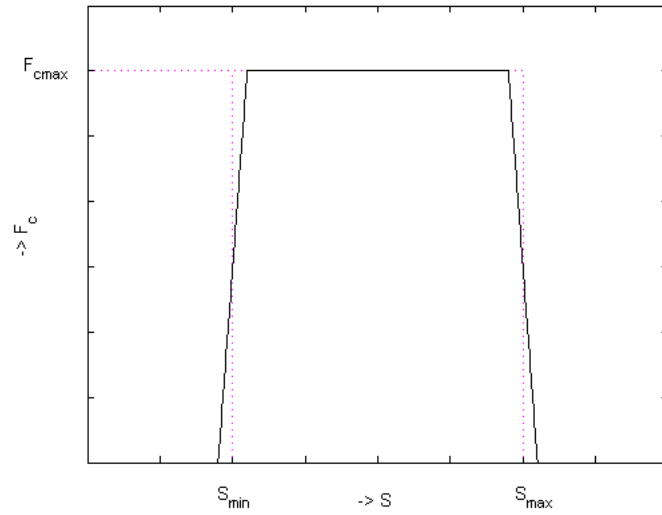
Figure A.6: The differentiation rate of chondrocytes as function of the stimulus S. F_c reached the value F_{cmax} when $S_{min} < S < S_{max}$.
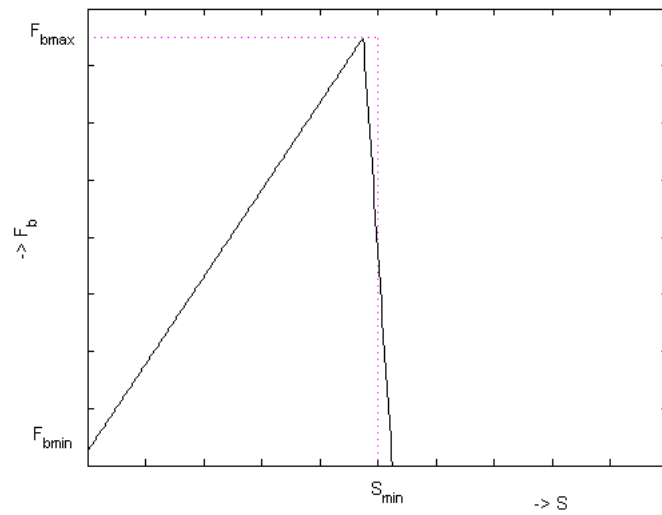
Figure A.7: The differentiation rate of osteoblasts as function of the stimulus S. Until the threshold S_{min} is reached by S, F_b increases when S does. After that F_b tends to zero.

Bibliography

[1] E. N. Marieb. *Human Anatomy and Physiology*, pages 175–201. Pearson Education Inc., international sixth edition, 2004.

[2] Picture from: http://www.orthop.washington.edu/userfiles/file/bankart.pdf.

[3] Picture from:http://www.readingshoulderunit.com/csra1/csra.htm.

[4] A. Bailon-Plaza and M. C. H Van der Meulen. A mathematical framework to study the effects of growth factors influences on fracture healing. *Journal of Theoretical Biology 212*, pages 191–209, 2001.

[5] Picture from: http://www.gla.ac.uk/ibls/fab/tutorial/generic/bone7.html.

[6] A. Andreykiv. *Simulation of Bone Ingrowth*. PhD thesis, TU Delft, 2006.

[7] http://wordnet.princeton.edu/perl/webwn?s=growth20factor.

[8] Ch. Ament and E. P. Hofer. A fuzzy logical model of fracture healing. *Journal of Biomechanics 33*, pages 961–968, 2000.

[9] J.A. Adam. A simplified model of wound healing (with particular reference to the critical size defect). *Mathematical and Computer Modelling 30*, pages 23–32, 1999.

[10] J.van Kan, A. Segal, and F. Vermolen. *Numerical Methods in Scientific Computing Part I: Modeling and discretisation*, page 98. VSSD, intermediate edition edition, 2004.

[11] P. Wesseling. Elements of computational fluid dynamics. 2002, 22-28.

[12] R. Huiskes, W. D. van Driel, P. J. Prendergast, and K. Søballe. A biomechanical regulatory model for periprosthetic fibrous-tissue differentiation. *Journal of materials science: Materials in medicine 8*, pages 785–788, 1997.

[13] J. Bear. *Dynamics of fluids in porous media.*, page 161. American Elsevier Publishing Company inc., New York, 1972.

[14] G. Aguilar, F. Caspar, F. Lisbona, and C. Rodrigo. Numerical stabilization of biot's consolidation model by a perturbation on the flow equation. *International journal for numerical methods in engineering*, pages 1–6, 2000.

[15] M. A. Bhatti. *Advanced Topics in Finite Element Analysis of Structures*, pages 24–25. John Wiley and Sons, 1st edition edition, 2006.

[16] A. Segal. Finite element methods for the incompressible navier-stokes equations. 2006.